(2)

NUMERICAL SOLUTION OF THREE-DIMENSIONAL UNSTEADY VISCOUS FLOWS

ONR Grant No: N00014-89-J-1319

Progress Report for the Period

December 1, 1991 - May 31, 1992

Prepared by

Lakshmi N. Sankar
Professor, School of Aerospace Engineering
Georgia Institute of Technology, Atlanta, GA 30332

INTRODUCTION

The long term objective of the present effort is the development of solution techniques for direct numerical simulation of unsteady 3-D incompressible turbulent flows. The kinetic aspects of this problem are governed by a set of parabolic partial differential equations, which may be efficiently integrated by a variety of time marching schemes. The kinematic aspects of this flow such as the relationship between velocity and vorticity, and the relationship between velocity and pressure are governed by elliptic partial differential equations, which can be solved at any instance in time, only by iterative techniques. Direct and/or large eddy simulation of turbulent flows over submarine configurations, turbomachinery, pumps, ducts and other configurations of interest to the U. S. Navy require efficient solution methods for solving the governing equations.

The near term objective of the present research is to investigate and develop efficient time marching schemes for integrating the governing equations, and to evaluate the stability and accuracy of the schemes developed by studying a class of 2-D and 3-D unsteady external flows for which good quality experimental and analytical results are available.

WORK DONE DURING THE REPORTING PERIOD

During the reporting period, extension of the 2-D unsteady, incompressible viscous flow methodology was to three-dimensions was completed. A very general 3-D, incompressible flow solver capable of handling arbitrary curvilinear grids has been developed. The grid may move or deform with time, as will be the case, for example, for incompressible viscous flow past a spinning propeller. The scheme is third order accurate in space, and first or second order accurate in time.

This solver has been applied to the following cases:

a) Incompressible viscous flow past an ellipsoid at an angle of attack. This geometry was chosen because of the availability of existing experimental data.

b) Incompressible viscous flow through a 90 degree bend, of rectangular cross section.

c) A multi-grid scheme has also been implemented for acceleration of the iterative process at every time step. Preliminary results on a two grid sequence are encouraging.

The above results are discussed in detail, along with the complete mathematical and numerical formulation in the following two documents:

1. W. G. Park, "Numerical Solution of 3-D Unsteady Incompressible Viscous Flows," Ph. D. Thesis Proposal, to be presented to the Thesis Committee in August 1992.

2. W. G. park and L. N. Sankar, " A Technique for the Prediction of Unsteady Incompressible Viscous Flows," Abstract submitted to the AIAA Aerospace Sciences Meeting in Reno, Nevada 1992.

Copies of the above two documents are enclosed.

ANTICIPATED RESULTS FOR THE NEXT REPORTING PERIOD

By the conclusion of the next reporting period (November 30, 1991), we plan to have the following case completed:

a) Viscous flow over a highly twisted tapered spinning propeller in forward motion. An SR-7 propeller (developed for aircraft applications) is being used for the code validation. But the flow solver can handle marine propeller configurations as well.

TECHNOLOGY TRANSFER

Dr. Wei Tang of the Naval Research center at Annapolis, Maryland (Phone: 301-267-2730) has acquired a version of our 2-D unsteady incompressible flow solver, and plans to extend it to flow through multi-stage turbine and compressor configurations. We hope to assist her in the validation of the flow solver, as needed.

APPENDIX

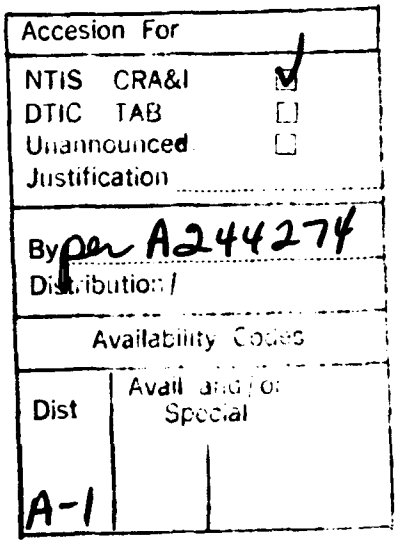

Numerical Solution of Three-Dimensional Unsteady Incompressible Viscous Flows

A Thesis Proposal

Presented to

The Faculty of the Division of Graduate Studies

By

Warn-Gyu Park

In Partial Fulfillment

of the Requirements for the Degree

Doctor of Philosophy

in the School of Aerospace Engineering

Georgia Institute of Technology

June 1992

LIST OF CONTENTS

CHAPTER I

INTRODUCTION

The accurate computation of three-dimensional unsteady incompressible flow problem is one of great interest to researchers working in fields of aerodynamics, hydrodynamics and biofluid mechanics. The flow over complex submarine shapes, flow past underwater propeller, flow within turbomachinery, and flow in blood vessels with compliant walls are examples of such flows. Accurate and efficient computation of such flows at high Reynolds numbers is presently not possible due to the mixed (elliptic-parabolic) nature of the governing equations. Indeed, methods for three-dimensional incompressible flows lag behind three-dimensional compressible flows by several years. Until accurate and efficient methods for three-dimensional incompressible, unsteady flows become available, it will not be possible to attempt challenging problems such as the first principles based on direct simulation or large eddy simulation of turbulent flows over complex geometries. The lack of such tools is one of the principal reasons that the first principles based prediction of turbulent flows past and through complex configurations has not been extensively attempted to date.

As Gresho and Sani (ref.1) pointed out, the pressure is a somewhat mysterious quantity in incompressible flows. It is not a thermodynamic variable since there is no 'equation of state' for an incompressible fluid. It is in one sense a mathematical artefact - a Lagrange multiplier that constrains the velocity field to remain divergence-free ; i.e. incompressible - yet its gradient is a relevant physical quantity ; a force per unit volume. It propagates at infinite speed in order to keep the flow always and everywhere incompressible ; i.e. it is always in equilibrium with a time-varying divergence-free velocity field.

One might have the idea that the compressible Navier-Stokes equation solvers can compute incompressible flows using compressible flow methods, and setting the Mach

number to be very low. But this idea becomes impractical at very low Mach numbers because the compressible Navier-Stokes equation solvers have a singular behavior as the Mach number approaches zero. This leads to an ill-conditioned stiff system of equations and consequently very slow convergence, or even divergence of the solution with time. This stiffness can be explained as a time step limitation (ref.2). We note that all explicit methods for solving the compressible Navier-Stokes equations are limited to a time step which is less than that given by the CFL condition. For example, in two-dimensions :

$$\Delta t \le \frac{1}{(|u|/\Delta x)+(|v|/\Delta y)+a\left[(1/\Delta x)^2+(1/\Delta y)^2\right]^{1/2}} \qquad (1.1)$$

where a is the speed of sound. From this condition, we observe that Δt approaches zero as the speed of sound approaches infinity. As a result, an "infinite" amount of computer time would be required to compute a truly incompressible flow in this manner. Implicit methods will permit a larger Δt , but the maximum value is normally less than 100 times that given by Eq.(1.1) because of truncation errors, approximate factorization errors, and so on. Thus, even if an implicit scheme is used, it is not practical to compute a truly incompressible Navier-Stokes solution using compressible flow methods.

The significant difficulty in solving incompressible Navier-Stokes equations is that the governing equations are a mixed elliptic-parabolic type of partial differential equations The continuity equation does not have a time derivative term and is given in the form of a divergence-free constraint. This is another major difference between the incompressible and compressible Navier-Stokes equations. The absence of a time derivative term in the continuity equation prohibits time integration of continuity equation by a time marching scheme. The compressible Navier-Stokes equations, on the other hand,are efficiently integrated by time marching schemes because they are a set of parabolic partial differential equations.

One of the commonly used approaches for solving two-dimensional incompressible flow is the vorticity-velocity or vorticity-stream function formulation (ref. 3,4,5). This is very efficient for two-dimensional problems, but this approach can not be extended straightforwardly to three dimensions. Consequently, the incompressible Navier-Stokes equations for three-dimensional problem are normally solved in their primitive variable form (p,u,v,w). Most methods using primitive variables may be classified into three groups. The first approach is the pressure Poisson method or Marker-and-Cell (MAC)

method which was first introduced by Harlow and Welch (ref.6). In the pressure Poisson method, the velocity field is advanced in time by solving the momentum equations with a stable explicit or implicit time marching scheme. Then the pressure field is evaluated at each time step by solving a Poisson equation for pressure directly (ref.7) or iteratively (ref.8,9,10). The continuity equation is thus satisfied when the pressure field is computed implicitly. This Poisson equation for pressure is obtained by taking the divergence of the unsteady momentum equations. The main idea of the MAC method (ref.11,12), an alternative to solving a pressure Poisson equation, is that the pressure field is updated at each time step by adjusting the pressure by an amount proportional to the negative of the velocity divergence :

$$p_{i,j}^{k} - p_{i,j}^{k-1} = -\beta\,(\nabla\cdot\vec{V})^{k-1} \qquad (1.2)$$

Here the superscripts 'k' and 'k-1' denote the iteration level, and β is a relaxation factor. Usually, a staggered grid system (ref.6) is used for the MAC method, because such a grid does not require the specification of pressure on the boundaries and does not produce unphysical oscillations in the pressure and velocity fields due to the central differencing of the pressure gradient term. The second approach is a projection method (or, fractional step method) which was first introduced by Chorin (ref.13). At the first step, an intermediate velocity is computed from the momentum equation without the pressure gradient term. Then a pressure field is computed which will make the velocity field obtained from the first fractional step divergence free. Finally, a second fractional step is performed using the pressure field just computed. The third group is the pseudocompressibility method (ref.14,15) which was also first introduced by Chorin (ref.16) primarily for obtaining steady state solutions. In this method, an artificial pressure derivative with respect to time is appended to the continuity equation. The entire system of equation is solved by a time marching scheme developed for compressible flows, such as the approximate factorization scheme (ref.17). If only a steady state is of interest, then the added pressure derivative drops out in the steady state, and physically correct solutions are achieved. If the aim is to achieve time-accurate calculations, either the artificial pressure derivative should be kept very small (which makes the equations extremely stiff, and forces very small time steps) or an inner iterative loop within each time step should be used (ref.18,19). A concept similar to the pseudocompressibility method, known as the penalty function method (ref.20) is widely used in the finite-element based incompressible flow solvers, which solves for p to satisfy :

$$\lambda p + \nabla \cdot \overline{V} = 0 \qquad (1.3)$$

In this method, the pressure gradient term of momentum equation is eliminated by substituting Eq.(1.3) into the momentum equation, and then solving the momentum equations with $\lambda \rightarrow 0$.

The methods for solving incompressible viscous flow discussed above have several drawbacks :

a) Most of them are only second order accurate in space, and first or second order accurate in time. Before these schemes can be applied to phenomena such as direct numerical simulation of turbulence, it will be necessary to raise the spatial and temporal accuracy to fourth or higher order.

b) The iterative convergence of the pressure Poisson solvers deteriorates at high Reynolds numbers.

c) In some instance (e.g. in the pseudocompressibility method), a trade off exists between temporal accuracy and convergence speed.

d) These methods do not take advantage of the vast progress that has been achieved in the solution of steady, viscous flows. For example, with rare exceptions, multigrid acceleration of Poisson solvers has not been attempted. Acceleration of the iterative solution of the pressure field to convergence using spatially varying time steps and grid sequencing have also not been extensively used.

e) There has been a growing interest in the use of massively parallel computer architectures such as the Connection Machine to solve unsteady viscous flows. Many of the compressible flow algorithms have already been adapted for use on these machines. There is a need to develop new procedures and modify existing algorithms for incompressible flows, on parallel machines.

The **objective** of this study is to develop an efficient and accurate solution technique for the analysis of two- and three-dimensional, unsteady, incompressible, viscous flows. The key features of the present scheme are listed below :

a) The primitive variables (p,u,v,w) are the primary unknowns in the present formulation.

b) The equations and the solution procedures are cast into a curvilinear, time-deforming coordinate system to handle complex internal and external flows.

c) An iterative time-marching scheme is used.

d) The present scheme is semi-implicit at each iteration and is suitable for efficient execution on the current generation of vector or massively parallel computer architectures.

e) The solution procedure works for a wide range of Reynolds numbers, with no appreciable loss in solution efficiency.

f) The present scheme is first order accurate in time and second order accurate in space, but higher order accuracy in space and time is easily achievable.

Only laminar flow is considered in the results to be discussed because the goal of this study is to develop an efficient and accurate incompressible Navier-Stokes solver. This method is however capable of handling turbulent flows provided a suitable turbulence model is used, and there are no inherent limitations in this method that will restrict it to laminar flows.

CHAPTER II

MATHEMATICAL FORMULATION

In this chapter, the governing equation for three-dimensional, unsteady, incompressible, viscous flow are presented in terms of the primitive variables (p,u,v,w) in both the Cartesian coordinate system and a curvilinear non-orthogonal, time deforming coordinate system.

2.1 Governing Equations in the Physical Domain

The motion of an incompressible viscous flow is governed by the conservation of mass and momentum, so called the continuity equation and the Navier-Stokes equation. Three-dimensional unsteady, incompressible, laminar, Navier-Stokes equations in an inertial Cartesian coordinate system may be written in a non-dimensional form as follows :

$$\frac{\partial q}{\partial t} + \frac{\partial}{\partial y}(E - E_v) + \frac{\partial}{\partial y}(F - F_v) + \frac{\partial}{\partial z}(G - G_v) = 0 \qquad (2.1)$$

where

$$q = \begin{bmatrix} 0 \\ u \\ v \\ w \end{bmatrix} \quad ; \quad E = \begin{bmatrix} u \\ u^2 + p \\ uv \\ uw \end{bmatrix} \quad ; \quad F = \begin{bmatrix} v \\ uv \\ v^2 + p \\ vw \end{bmatrix} \quad ; \quad G = \begin{bmatrix} w \\ uw \\ vw \\ w^2 + p \end{bmatrix} \qquad (2.2)$$

$$E_v = \frac{1}{Re}\begin{bmatrix} 0 \\ \tau_{xx} \\ \tau_{xy} \\ \tau_{xz} \end{bmatrix} \quad ; \quad F_v = \frac{1}{Re}\begin{bmatrix} 0 \\ \tau_{yx} \\ \tau_{yy} \\ \tau_{yz} \end{bmatrix} \quad ; \quad G_v = \frac{1}{Re}\begin{bmatrix} 0 \\ \tau_{zx} \\ \tau_{zy} \\ \tau_{zz} \end{bmatrix}$$

The stress terms are given by

$$
\begin{aligned}
\tau_{xx} &= \frac{2}{3}\left(2\frac{\partial u}{\partial x} - \frac{\partial v}{\partial y} - \frac{\partial w}{\partial z}\right) \\
\tau_{yy} &= \frac{2}{3}\left(2\frac{\partial v}{\partial y} - \frac{\partial u}{\partial x} - \frac{\partial w}{\partial z}\right) \\
\tau_{zz} &= \frac{2}{3}\left(2\frac{\partial w}{\partial z} - \frac{\partial u}{\partial x} - \frac{\partial v}{\partial y}\right) \\
\tau_{xy} &= \tau_{yx} = \frac{\partial u}{\partial y} + \frac{\partial v}{\partial x} \\
\tau_{xz} &= \tau_{zx} = \frac{\partial w}{\partial x} + \frac{\partial u}{\partial z} \\
\tau_{yz} &= \tau_{zy} = \frac{\partial v}{\partial z} + \frac{\partial w}{\partial y}
\end{aligned}
\tag{2.3}
$$

In Eq.(2.2) and Eq.(2.3), u, v and w are the normalized Cartesian components of velocity, p is the normalized pressure, and Re is the Reynolds number defined as :

$$
\mathrm{Re} = \frac{\rho V_\infty L}{\mu} \tag{2.4}
$$

where ρ, V_∞, L and μ are fluid density, freestream velocity, reference length and coefficient of viscosity (dynamic viscosity), respectively.

The governing equation (2.1) is a mixed set of elliptic-parabolic partial differential equations. As mentioned before, the absence of a time derivative in continuity equation and the absence of an explicit relationship between pressure and divergence-free condition on the velocity prohibit time integration in a straightforward manner by a stable time marching scheme. In this study, the continuity equation is modified to directly link the iterative changes in pressure to changes in velocity, as done in the Marker-and-Cell method.

2.2 Governing Equations in the Computational Domain

If the above equations are directly used on a Cartesian system to flow past complex geometries, the imposition of boundary conditions will require a complicated interpolation of the data on local grid lines, since the computational boundaries of complex geometries do not coincide with coordinate lines.This leads to a local loss of accuracy in the computed solution and leads to a complex program. To avoid these difficulties, a transformation from the physical domain (Cartesian coordinates(t,x,y,z)) to computational domain (generalized curvilinear coordinates(τ,ξ,η,ζ)) is used. After transformation from the physical domain to the computational domain, the governing equations can be written as :

$$\frac{\partial \hat{q}}{\partial \tau}+\frac{\partial}{\partial \xi}\left(\hat{E}-\hat{E}_v\right)+\frac{\partial}{\partial \eta}\left(F-\hat{F}_v\right)+\frac{\partial}{\partial \zeta}\left(G-\hat{G}_v\right)=0 \tag{2.5}$$

where

$$\hat{q}=\frac{1}{J}\begin{bmatrix}0\\u\\v\\w\end{bmatrix}$$

$$\hat{E}=\frac{1}{J}\begin{bmatrix}U-\xi_t\\uU+p\xi_x\\vU+p\xi_y\\wU+p\xi_z\end{bmatrix}\;;\;\hat{F}=\frac{1}{J}\begin{bmatrix}V-\eta_t\\uV+p\eta_x\\vV+p\eta_y\\wV+p\eta_z\end{bmatrix}\;;\;\hat{G}=\frac{1}{J}\begin{bmatrix}W-\zeta_t\\uW+p\zeta_x\\vW+p\zeta_y\\wW+p\zeta_z\end{bmatrix} \tag{2.6}$$

and

$$\hat{E}_v=\frac{1}{J\,Re}\begin{bmatrix}0\\(\nabla\xi\cdot\nabla\xi)u_\xi+(\nabla\xi\cdot\nabla\eta)u_\eta+(\nabla\xi\cdot\nabla\zeta)u_\zeta\\(\nabla\xi\cdot\nabla\xi)v_\xi+(\nabla\xi\cdot\nabla\eta)v_\eta+(\nabla\xi\cdot\nabla\zeta)v_\zeta\\(\nabla\xi\cdot\nabla\xi)w_\xi+(\nabla\xi\cdot\nabla\eta)w_\eta+(\nabla\xi\cdot\nabla\zeta)w_\zeta\end{bmatrix}$$

$$\hat{F}_v=\frac{1}{J\,Re}\begin{bmatrix}0\\(\nabla\eta\cdot\nabla\xi)u_\xi+(\nabla\eta\cdot\nabla\eta)u_\eta+(\nabla\eta\cdot\nabla\zeta)u_\zeta\\(\nabla\eta\cdot\nabla\xi)v_\xi+(\nabla\eta\cdot\nabla\eta)v_\eta+(\nabla\eta\cdot\nabla\zeta)v_\zeta\\(\nabla\eta\cdot\nabla\xi)w_\xi+(\nabla\eta\cdot\nabla\eta)w_\eta+(\nabla\eta\cdot\nabla\zeta)w_\zeta\end{bmatrix}$$

$$\hat{G}_v=\frac{1}{J\,Re}\begin{bmatrix}0\\(\nabla\zeta\cdot\nabla\xi)u_\xi+(\nabla\zeta\cdot\nabla\eta)u_\eta+(\nabla\zeta\cdot\nabla\zeta)u_\zeta\\(\nabla\zeta\cdot\nabla\xi)v_\xi+(\nabla\zeta\cdot\nabla\eta)v_\eta+(\nabla\zeta\cdot\nabla\zeta)v_\zeta\\(\nabla\zeta\cdot\nabla\xi)w_\xi+(\nabla\zeta\cdot\nabla\eta)w_\eta+(\nabla\zeta\cdot\nabla\zeta)w_\zeta\end{bmatrix} \tag{2.7}$$

with the contravariant velocities U, V and W :

$$\begin{aligned}U&=\xi_t+u\xi_x+v\xi_y+w\xi_z\\V&=\eta_t+u\eta_x+v\eta_y+w\eta_z\\W&=\zeta_t+u\zeta_x+v\zeta_y+w\zeta\end{aligned} \tag{2.8}$$

Here J is the Jacobian of transformation

$$J = \frac{\partial(\xi,\eta,\zeta)}{\partial(x,y,z)} = \frac{1}{\begin{vmatrix} x_\xi & x_\eta & x_\zeta \\ y_\xi & y_\eta & y_\zeta \\ z_\xi & z_\eta & z_\zeta \end{vmatrix}} \tag{2.9}$$

The quantities ξ_t , η_t and ζ_t are presented if the grid is in motion (as in the case of flow past an oscillating airfoil or a spinning propeller). These quantities are given in terms of the velocity of the grid (x_τ, y_τ, z_τ) with reference to a stationary observers :

$$\begin{aligned} \xi_t &= - x_\tau \xi_x - y_\tau \xi_y - z_\tau \xi_z \\ \eta_t &= - x_\tau \eta_x - y_\tau \eta_y - z_\tau \eta_z \\ \zeta_t &= - x_\tau \zeta_x - y_\tau \zeta_y - z_\tau \zeta_z \end{aligned} \tag{2.10}$$

CHAPTER III

NUMERICAL FORMULATION

The numerical procedure for solving the governing equation is an iterative time marching scheme which attempts to solve the discretized form of equations to a user-specified accuracy at any time step. Details of the iterative process are given in this chapter.

3.1 Grid Generation

The present method is a finite difference scheme which solves the discretized form of the partial differential equations at a set of discrete points in the flow field. Therefore, a set of grid points within the domain, including its boundaries, must be specified before solving the governing equations. Such a body-fitted grid system may be generated by conformal mapping, by algebraic method, or by partial differential equation techniques. In this study, body-fitted C-grid (Fig.1) and H-O grid system (Fig.5) are generated by an algebraic method for two-dimensional flow around NACA 0012 airfoil and three-dimensional flow around the ellipsoid of revolution, respectively. For the three-dimensional curved duct problem, a sheared/rotated Cartesian grid is used.

3.2 Grid Motion

In unsteady state computations, it is convenient to use a moving grid to account for the body motion. The grid is attached to the body and it rotates or translate with the body. The grid coordinates can be advanced explicitly by a first order time marching scheme :

$$\begin{aligned} x^{n+1} &= x^n + x_\tau^n \, \Delta t \\ y^{n+1} &= y^n + y_\tau^n \, \Delta t \\ z^{n+1} &= z^n + z_\tau^n \, \Delta t \end{aligned} \qquad (3.1)$$

However, if only a pure rotational motion is considered (say in a two-dimensional flow problem), new coordinates of grid at any instance in time can be simply obtained by using the following relations :

$$\begin{bmatrix} x \\ z \end{bmatrix} = \begin{bmatrix} \cos\theta & -\sin\theta \\ \sin\theta & \cos\theta \end{bmatrix} \begin{bmatrix} x' \\ z' \end{bmatrix} \tag{3.2}$$

where (x, z) is the instantaneous x, z values of the node and (x', z') is the x, z values of the node prior to rotation, and θ is the clockwise rotation angle. In such a case x_τ and z_τ may be found by analytical differentiation of (3.2) with respect to time or from (3.1).

3.3 Iterative Time Marching Procedure

The goal of the present procedure is to advance the flow properties (p,u,v,w) from a known time level 'n' to the next time level 'n+1'. First of all, let us consider the momentum equation. Since the momentum equation is a parabolic type of partial differential equation, it can be solved using a time marching scheme as follows :

$$\frac{1}{\Delta\tau}\left(\bar{q}^{n+1} - \bar{q}^{n}\right) + \delta_\xi \bar{E}^{n+m} + \delta_\eta \bar{F}^{n+m} + \delta_\zeta \bar{G}^{n+m} = \delta_\xi \bar{E}_v^{n+m} + \delta_\eta \bar{F}_v^{n+m} + \delta_\zeta \bar{G}_v^{n+m} \tag{3.3}$$

where $\bar{q}$ is $\hat{q}$ of Eq.(2.6) excluding the first row element, i.e.,

$$\bar{q} = \frac{1}{J}\begin{bmatrix} u \\ v \\ w \end{bmatrix} \tag{3.4}$$

Similarly, $\bar{E}$, $\bar{F}$, $\bar{G}$, $\bar{E}_v$, $\bar{F}_v$ and $\bar{G}_v$ can be also defined. For example,

$$\bar{E} = \begin{bmatrix} uU + p\xi_x \\ vU + p\xi_y \\ wU + p\xi_z \end{bmatrix} \tag{3.5}$$

The above discretization of Eq(3.3) is first order accurate in time if 'm' is zero or one, and second order accurate if 'm' is set to 1/2. The operators, δ_ξ, δ_η and δ_ζ represent second order accurate or higher order accurate spatial differences. The higher order spatial accuracy may be achieved on uniform grids using Pade approximations to the derivatives; on highly stretched grids, higher order accuracy may be achieved using a Lagrangean fit to the flow variables. In high Reynolds number flows, the Lagrangean fit need not be equally weighted about the node, but may be biased in the direction of flow. For example, when the flow is from left to right, if the Lagrangean interpolation of flow variables is done using nodes only to the left of, and including, the current node, then an upwind formulation results.

If the Newton iteration method is applied to solve this unsteady flow problem, Eq.(3.3) is rewritten as follows :

$$\frac{1}{\Delta\tau}\left(\bar{q}^{n+1,\,k+1}-\bar{q}^{n}\right)+\delta_\xi\bar{E}^{n+m,\,k+1}+\delta_\eta\bar{F}^{n+m,\,k+1}+\delta_\zeta\bar{G}^{n+m,\,k+1}= \delta_\xi\bar{E}_v^{n+m,\,k+1}+\delta_\eta\bar{F}_v^{n+m,\,k+1}+\delta_\zeta\bar{G}_v^{n+1,\,k+1} \tag{3.6}$$

Following a local linearization of $\bar{E}$, $\bar{F}$, $\bar{G}$, $\bar{E}_v$, $\bar{F}$ and $\bar{G}_v$ about the 'n+m' time level and at the 'k' iteration level, one may have

$$\left(I+\frac{\partial}{\partial\xi}A+\frac{\partial}{\partial\eta}B+\frac{\partial}{\partial\zeta}C\right)\Delta\bar{q}=\omega\,\bar{R}^{n+m,\,k} \tag{3.7}$$

where ω is a relaxation factor and A, B and C are the Jacobian matrices of the flux vectors $\bar{E}-\bar{E}_v$, $\bar{F}-\bar{F}_v$ and $\bar{G}-\bar{G}_v$, respectively:

$$A=\frac{\partial(\bar{E}-\bar{E}_v)}{\partial\bar{q}} \quad ; \quad B=\frac{\partial(\bar{F}-\bar{F}_v)}{\partial\bar{q}} \quad ; \quad C=\frac{\partial(\bar{G}-\bar{G}_v)}{\partial\bar{q}} \tag{3.8}$$

and $\bar{R}^{n+m,\,k}$ is the residual vector, defined as :

$$\bar{R}^{n+m,\,k}=-\frac{\bar{q}^{n+1,\,k}-\bar{q}^{n}}{\Delta\tau}-\left(\delta_\xi\bar{E}^{n+m,\,k}+\delta_\eta\bar{F}^{n+m,\,k}+\delta_\zeta\bar{G}^{n+m,\,k}\right) +\left(\delta_\xi\bar{E}_v^{n+m,\,k}+\delta_\eta\bar{F}_v^{n+m,\,k}+\delta_\zeta\bar{G}_v^{n+m,\,k}\right) \tag{3.9}$$

Note that when $\overline{R}^{n+m,\,k}$ goes to zero, the momentum equations in their discretized form are exactly satisfied, and the solution is independent of ω, and any approximations made in the construction of A, B and C.

Next, let's consider the continuity equation. As mentioned in Chapter I, in order to solve incompressible viscous flow problems efficiently, we need a relationship coupling changes in the velocity field with changes in the pressure field while satisfying the divergence-free constraint. In the present study, the Marker-and-Cell (MAC) approach is used to link the iterative changes between them, and can be written :

$$\Delta p = -\beta\,(\nabla \cdot V)^{n+1,\,k} \tag{3.10}$$

where $\Delta p = p^{n+1,\,k+1} - p^{n+1,\,k}$

and β is a relaxation factor,that may even vary from node to node using local time concept. Again, when Δp goes to zero, the continuity equation is exactly satisfied at each time step, even in unsteady flows.

In curvilinear coordinate system, Eq.(3.10) can be rewritten as :

$$\Delta\left(\frac{p}{J}\right) = -\beta\left[\frac{\partial}{\partial\xi}\left(\frac{U-\xi_t}{J}\right)+\frac{\partial}{\partial\eta}\left(\frac{V-\eta_t}{J}\right)+\frac{\partial}{\partial\zeta}\left(\frac{W-\zeta_t}{J}\right)\right]^{n+1,\,k} \tag{3.11}$$

The contravariant velocities, U, V and W are already defined in Eq.(2.8).

Eq.(3.10) states that if a cell is accumulating mass, then the pressure value at next iteration is increased to repel fluid away from the cell. If a cell is losing mass, then the pressure value is lowered to draw fluid. Thus the pressure field is iteratively updated along with the velocity field until the conservation of mass is satisfied.

Combining the momentum equation, Eq.(3.7) and the continuity equation, Eq.(3.11) , and applying the numerical discretization in time and space at all nodes in the flow field, a system of simultaneous equation results for the quantity $\Delta\hat{q}$ equal to $\left(\Delta\frac{p}{J}, \Delta\frac{u}{J}, \Delta\frac{v}{J}, \Delta\frac{w}{J}\right)$. This system may be formally written as :

$$[M]\{\Delta\hat{q}\} = \{R\} \tag{3.12}$$

Here, since the right hand side is the discretized form of the unsteady governing equations, as long as $\{\Delta\hat{q}\}$ is driven to zero, the discretized form of unsteady Navier-Stokes equations are exactly satisfied at physical time level 'n+1'.

Although the matrix [M] is a sparse, banded matrix, direct inversion of this matrix requires a huge number of arithmetic operations. A common strategy in iterative solutions of elliptic equations is to approximate the matrix [M] by another, easily inverted matrix [N]. The closer the matrix [N] is to [M], the faster the iterative convergence of the solution at any time step. In this study, matrix [N] contains only the diagonal contributions of matrix [M], and Eq.(3.12) becomes an explicit form which is easier to be tailored for efficient execution on the current generation of vector or massively parallel computer architectures than an implicit form. This simplicity comes at the expense of the iterative speed. Acceleration of the iterative process above is a major contribution of this work to the state of the art.

The spatial derivatives of convective flux terms are differenced by using third order accurate upwind QUICK (Quadratic Upstream Interpolation for Convective Kinematics, ref.21) scheme to reduce unphysical oscillations or false diffusion for high Reynolds number flows, and the spatial derivatives of viscous terms are differenced using half-point central differencing. The spatial derivatives of continuity equation is differenced with central differencing and a fourth order artificial damping term is added to the continuity equation to stabilize the present procedure. The QUICK scheme is constructed that, instead of such a linear interpolation for the convective terms as used in standard one-sided differencing schemes, a three-point upstream weighted quadratic interpolation is used. For example, let's consider the convective term in ξ-direction which may be approximated as follows :

$$\frac{\partial}{\partial\xi}\left(\frac{uU}{J}\right)=\frac{1}{\Delta\xi}\left[\left(\frac{uU}{J}\right)_{i+\frac{1}{2}}-\left(\frac{uU}{J}\right)_{i-\frac{1}{2}}\right] \tag{3.13}$$

where

$$\left(\frac{uU}{J}\right)_{i+\frac{1}{2}}=\left(\frac{U}{J}\right)_{i+\frac{1}{2}}\left\{\frac{(u_{i+1}+u_i)}{2}-\frac{\Delta\xi^2}{8}\,CURV_{i+\frac{1}{2}}\right\}$$
$$\left(\frac{uU}{J}\right)_{i-\frac{1}{2}}=\left(\frac{U}{J}\right)_{i-\frac{1}{2}}\left\{\frac{(u_{i-1}+u_i)}{2}-\frac{\Delta\xi^2}{8}\,CURV_{i-\frac{1}{2}}\right\} \tag{3.14}$$

The curvature terms (CURV) depend on the direction of the contravariant velocity U :

$$CURV_{i+\frac{1}{2}} = \begin{cases} \frac{1}{\Delta\xi^2}\left(u_{i+1} - 2u_i + u_{i-1}\right) & \text{if } U_{i+\frac{1}{2}} > 0 \\ \frac{1}{\Delta\xi^2}\left(u_{i+2} - 2u_{i+1} + u_i\right) & \text{if } U_{i+\frac{1}{2}} < 0 \end{cases} \tag{3.15}$$

$$CURV_{i-\frac{1}{2}} = \begin{cases} \frac{1}{\Delta\xi^2}\left(u_i - 2u_{i-1} + u_{i-2}\right) & \text{if } U_{i-\frac{1}{2}} > 0 \\ \frac{1}{\Delta\xi^2}\left(u_{i+1} - 2u_i + u_{i-1}\right) & \text{if } U_{i-\frac{1}{2}} < 0 \end{cases} \tag{3.16}$$

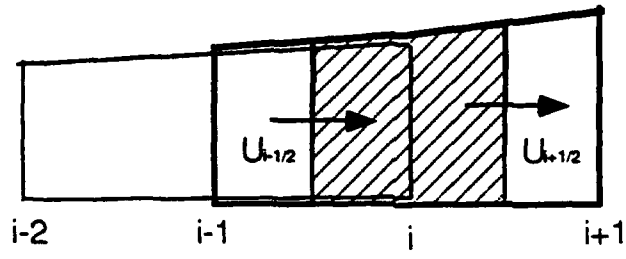

(a)

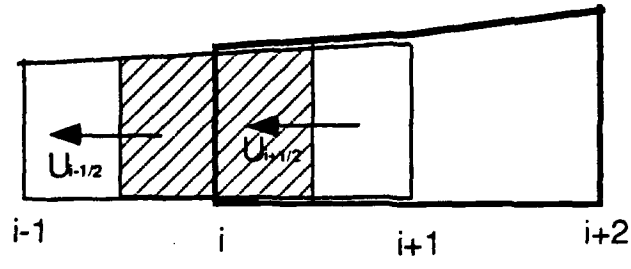

(b)

Fig. 3.1. Quadratic upstream interpolation
(a) For U > 0
(b) For U < 0

3.4 Initial and Boundary Conditions

The governing equation (2.1) and (2.5) is a mixed elliptic-parabolic type of partial differential equation, and requires initial conditions to start the calculation as well as

boundary condition at every time step. The parabolic nature of the flow ensures that the flows will be independent of initial conditions, after large number of time step.

In the present work, the quantities Δp, Δu, Δv and Δw are set to zero at all solid and fluid boundaries. The boundary conditions are updated after every interior points updated during each iteration. Thus the boundary values as well as interior values are iteratively advanced from a time level 'n' to 'n+1'.

Initial Conditions :

In the case of external flows, we assume that the object is impulsively started from rest . Therefore, the uniform freestream conditions are used as initial conditions. In the case of internal flows, parallel flow solutions (e.g. Poiseulle flow in a square duct) are used to start the calculations.

Farfield Boundary Conditions :

For external flow applications, the farfield boundary is placed far away from the solid surface. Thus, it is natural to specify the freestream values at the farfield boundaries except along the outflow boundary where the extrapolation for velocities in combination with $p = p_\infty$ is used, to account for the removal of vorticity from the flow domain by convective process.

Boundary Conditions on the Solid Surface :

On the solid surface, the no slip condition is imposed for velocity components. The surface pressure distribution is determined by solving the normal gradient of pressure to be zero :

$$\frac{\partial p}{\partial n} = 0 \tag{3.17}$$

Some researchers (ref.22, 23) obtain the boundary conditions for pressure from the normal component of momentum equation at the wall

$$\frac{\partial p}{\partial n} = \frac{1}{Re} \frac{\partial^2 u_n}{\partial n^2} \tag{3.18}$$

where u_n is the normal component of velocity. In high Reynolds number flows, the viscous stress contribution to the normal momentum equation can be neglected at the wall and the grid point adjacent to the surface will be sufficiently fine so that constant pressure normal to the surface can be assumed. Thus Eq.(3.17) is an acceptable boundary condition.

Boundary Conditions on the Cut and Singular Line :

Since the C-grid and the H-O grid which are used for two-dimensional airfoil problem and three-dimensional body of revolution have a cut and singularlines, respectively, special treatment is needed (see Fig. 3.2 and 3.3). Across the cut of the C-grid system, flow quantities should be continuous. The flow quantities on the cut can be obtained by averaging the flow properties from above and below the cut. On the singular lines that occur in a H-O grid system, the flow quantities are obtained by extrapolating from two adjacent interior points and then averaging them azimuthally to ensure that the flow quantities are singe-valued.

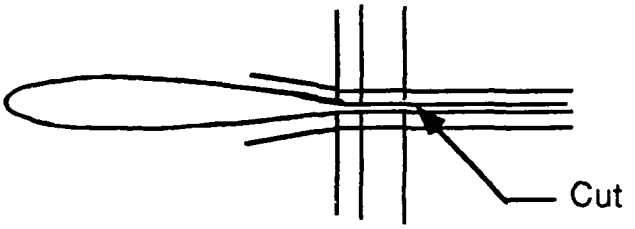

Fig.3.2 Cut of the C-grid system

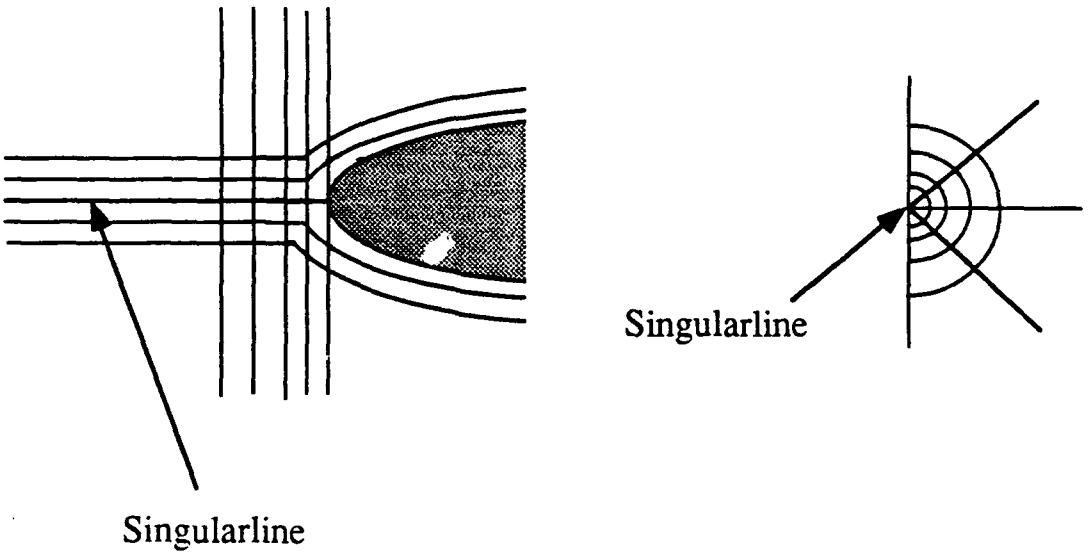

Fig.3.3. Singularline of the H-O grid system

3.5 Acceleration by Multigrid Technique

Since the matrix [N] (which is an approximate to matrix [M] of Eq.(3.12)) is a simple diagonal-matrix, it leads to slow convergence of the pressure and velocity fields at every time step. Use of such a simple diagonal matrix simplifies the inversion, and makes the flow solver 100% vectorizable and parallelizable. To accelerate the present procedure, a multigrid technique (Coarse Grid Correction method) is applied in this study.

The principles behind the present multigrid technique are as follows. The quantities (Δu, Δv, Δw, Δp) may be viewed as Fourier series-like sums made of components of different wave lengths. An extremely coarse grid linking a point to a node several units away is effective in computing the long wave length components. A very fine grid is effective in computing the short wave length components, and is very inefficient for computing the long wave length components. The multigrid technique attempts to compute these individual components of Δq on grids of several levels efficiently. When the process converges, of course, the discretized equations (i.e. RHS of Eq.(3.7) and (3.11)) are exactly satisfied on the finest grid.

The coarse grid correction algorithm presently used (given here for 2-grid sequence for simplicity) is as follows :

i) Compute the residual $\{R\}$ appearing on the right hand side of Eq.(3.12) on the fine grid using $q^{n+1,k}$.

ii) Transfer the residual from the fine grid to the coarse grid using the injection operation, $I_h^{2h}R$. An injection operation is given at any node (i,j) in two-dimensional case by

$$I_h^{2h}R_{i,j} = R_{i,j} + \frac{1}{2}\left(R_{i+1,j} + R_{i-1,j} + R_{i,j+1} + R_{i,j-1}\right) + \frac{1}{4}\left(R_{i+1,j-1} + R_{i-1,j+1} + R_{i-1,j-1} + R_{i+1,j+1}\right) \tag{3.19}$$

iii) Compute the quantity Δq at every point on the coarse grid by solving the system of equation :

$$[N]\{\Delta q / J\} = \left\{I_h^{2h}R\right\} \tag{3.20}$$

iv) Interpolate the Δq values computed in step (iii) back on to the fine grid by using the bilinear interpolation.

v) Compute the updated values of the flow properties $q^{n+1,k+1}$ as $q^{n+1,k} + \Delta q$.

Repeat step (i) - (v) till Δq is driven to zero.

The present 2-D solver accepts grids upto 3 levels.

To the writer's knowledge, the multigrid technique in unsteady incompressible flows has been applied only to pressure-Poisson equation. The u-, v- and w- momentum equations are usually solved only on a single grid. The present work fully exploits the benefits of the multigrid method for all the equations, while keeping the form of the matrix [N] extremely simple. This allows use of larger time steps and improved convergence as discussed on Chapter IV. The present investigator applied a conjugate gradient like scheme, called the GMRES (Generalized Minimal Residuals) to solve Eq.(3.12). The matrix [N] was used as the preconditioner. The success of the GMRES scheme crucially depends on the closeness of [N] to [M]. That is the eigenvalues of the matrix $\left[I - N^{-1}M\right]$ must be small and closely packed. The use of GMRES with [N] as a preconditioner was not successful.

CHAPTER IV

RESULTS AND DISCUSSION

In this chapter, the work done to date is presented. To validate the present procedure, three cases were tested. The first test case is two-dimensional unsteady viscous flow over an oscillating airfoil. The second is three-dimensional steady flow over an ellipsoid of revolution. The third is the flow through a curved duct. Numerical results are presented in the form of instantaneous streamlines, velocity profiles, vorticity contours, surface pressure distribution, and aerodynamic loads. Streamlines and surface pressure distributions are compared with flow visualization and the other available numerical data .

4.1 Dynamic Stall of an Oscillating Airfoil

The computations were carried out for a sinusoidally pitching NACA 0012 airfoil, at Re = 5,000 and κ = 0.5, where κ is reduced frequency of oscillation,defined by

$$\kappa = \frac{\Omega c}{2 V_\infty} \tag{4.1}$$

where Ω is the radians of rotation per second and c is chord of airfoil. The physical interpretation of reduced frequency is the number of radians of oscillation per semi-chord length of travel. This case has been previously studied by Mehta (ref.3) at NASA Ames Research Center using a velocity-vorticity formulation and its flow visualization was carried out by Werlé (ref. 24) in ONERA.

After the flow is fully developed at zero angle of attack, the airfoil is allowed to oscillate in pitch through an angle of attack range from 0 degree to 20 degree given by $\alpha = 10^\circ(1 - \cos t)$. Fig.1 shows the body-fitted grid around the airfoil used in this study. Fig.2 shows the instantaneous streamlines (actually, called particle tracers in PLOT3D software), velocity profiles and vorticity contours at selected angle of attack. Fig.3 shows the surface pressure distribution. In general, the streamline patterns and surface pressure distributions are in very good agreement with flow visualization and Mehta's numerical

results except that the present procedure predicts a little earlier generation of vortex than Mehta's method. The flow visualizations were carried out with air bubble in the water tunnel. Here, we should note that photographs showing air bubble trajectories were taken at an exposure time of 1/10 seconds. Therefore, in unsteady flow the air bubble trajectories near the surface of airfoil represent neither streamlines nor streaklines because the pictures contain many paths over the exposure time. On the orther hand, the instantaneous streamline is a streamline at any instant of time, i.e. we assume the flowfield is frozen at any instant of time and draw the streamline. In other words, the instantaneous streamline is equivalent to the bubble trajectories with an infinitesimal exposure time. Thus, the flow visualization with air bubble is different from the instantaneous streamline, and should be used only for qualitative comparison. Fig.4 shows the lift, drag and moment hysteresis loops. The main feature of dynamic stall which is significantly different from static stall is due to the generation of a vortex near the leading edge. This vortex passes over the upper surface of airfoil, creating large variations in the aerodynamic forces and moment. From these figures, it is seen that the growth of lift during the upstroke is slow and gradual, well past the static-stall angle. The separation region, which is present over a small region near the trailing edge at first, moves upstream as the angle of attack increases. The pitching moment does not change much during the upstroke. The surface pressure distribution at an angle of attack of 18.6 degree shown in Fig.3 shows another pressure peak near the quarter chord. This indicates the leading-edge vortex is already generated, and this can be identified in Fig.2 (c). As the leading-edge vortex moves downstream, the chordwise surface pressure distribution and aerodynamic forces are significantly varied, especially during the downstroke. This variation may depend on the Reynolds number, airfoil shapes and reduced frequency. The moment stall, associated with an increase of negative moment, begins at about 18.5 degree in the downstroke.

4.2 3-D Steady Flow over an Ellipsoid of Revolution

To validate the capability of the present method to handle three-dimensional viscous flows, the present procedure was tested by computing the flow past a 6:1 ellipsoid of revolution at 10 degree angle of attack, at a Reynolds number of 5,000. Fig.5 shows the body-fitted grid system. Fig.6 shows streamlines over the body surface. There is a limited amount of experimental data (ref.25, 26) available for this particular configuration, at high Reynolds number ($Re=7.2 \times 10^6$). Fig.7 shows the surface pressure distribution on the windward and leeward sides of the symmetry plane, along with the experimental data.

Good agreement is evident everywhere except in the last 10% of the body, where the present laminar simulation predicts flow separation, and a flattening out of the pressure distribution.

4.3 3-D Steady Flow through a 90^0 Bended Square Duct

To validate the capability to handle three-dimensional internal flow problems, the flow within a square duct with a 90-deg bend was tested. The radius of curvature of the inner wall in the curved section is 1.8 times of the side length of square cross-section. This particular configuration (Fig.8) was experimented by Humphrey et al. (ref.27) at a Reynolds number of 790 based on the average inflow velocity and hydraulic diameter. The inflow and outflow velocity profile are obtained by solving the equation of fully developed duct flow (ref.28) :

$$\frac{\partial^2 u}{\partial y^2} + \frac{\partial^2 u}{\partial z^2} = \frac{1}{\mu}\frac{dp}{dx} = \text{const.} \qquad (4.2)$$

This equation is a standard form of Poisson equation and can be solved by ADI scheme. Fig.9 shows the streamwise velocity profiles compared with the experimental data of Humphrey et al. The plots on the left side of Fig.9 are at $y/y_{1/2} = 0.5$, which is midway between the left side wall and the symmetry plane of square duct and the right side plots are at $y/y_{1/2} = 0$, which is on the symmetry plane. The inside and outside wall are corresponding to $z = 0$ and $z = 1$, respectively. The results are in general good agreement with experiments except at $\theta = 90$deg. This discrepancy may be disappeared if a more fine grid is adopted. This will be further investigated. The present grid system is 61x21x21. In Fig.10, the cross-sectional velocity profiles are plotted at $\theta = 30$, 60 and 90 deg. The top side and bottom side of cross-section are the inside wall and outside wall, respectively. In this figure, the pair of secondary vortices is shown and these vortices are generated due to the pressure difference between the higher pressure on the outside wall and lower pressure on the inside wall. Fig.11 is a sideview of streamwise velocity profiles at $y/y_{1/2} = 0.5$ and $y/y_{1/2} = 0$. Fig.12 shows streamwise velocity profiles from a viewpoint which is located at upper 45° in the xz-plane. The plot at $z = 0.25$ is corresponding to the midway plane between the inside wall and the plane of symmetry. The plots at $z = 0.5$ and 0.75 are on the plane of symmetry and the midway between the outside wall and the symmetry plane, respectively.

4.4 Acceleration of 2-D Flow Solver by Multigrid Technique

The multigrid technique was implemented to the two-dimensional steady and unsteady solver. The fine grid system has (81x41) grid points and the coarse grid system has the half of the fine grid points, i.e. (41x21) grid points, and the coarsest grid system has (21x11) grid points. The two grid system consists of the fine and coarse grid system (Fig. 4.1.(a)) and the three grid system consists of all of them as shown in Fig.4.1.(b). Especially, three grid system such as Fig. 4.1.(b) is called V-cycle.

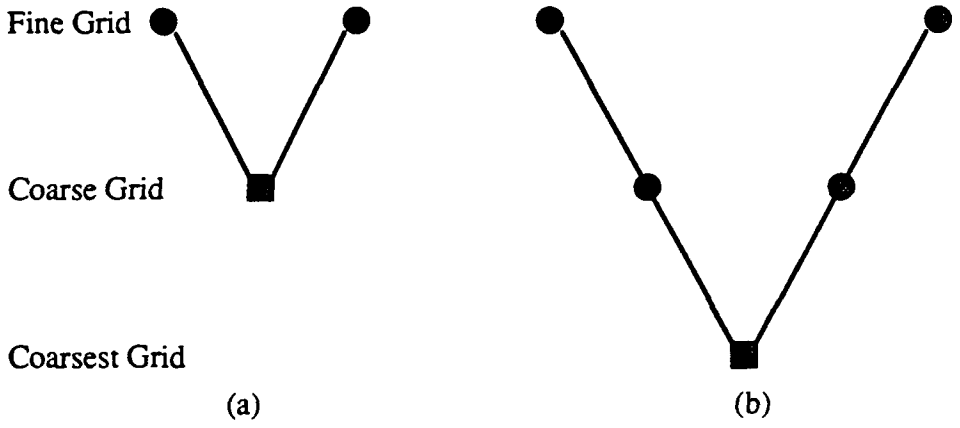

Fig. 4.1 Structure of multigrid cycle
(a) Two-grid system
(b) Three-grid system

Fig.13 shows the convergence history of the global residual (l_2-norm of RHS of Eq (3.12)) reduction in CPU time for steady flow over NACA 0012 airfoil at zero angle of attack. Upto 40% and 60% acceleration was obtained using two- and three-grid system, respectively. The CPU time is based on 25 iterations at each time step on an IBM RISC/6000 workstation. Fig.14 shows the history of global residual for sinusoidally oscillating airfoil (50 iterations/time step), where the three-grid system is used for multigrid. The residual by the multigrid technique maintains lower level than that of single grid iteration procedure indicating that the discretized equations are solved to much high levels of accuracy using the multigrid technique. The surface pressure distribution and

dynamic stall hysteresis is nearly the same as those of single grid system and are not plotted here.

CHAPTER V

PROPOSED WORK

An iterative procedure for two- and three-dimensional unsteady, incompressible, viscous flow has been developed. It has been applied to massively separated flow over oscillating airfoil, three-dimensional flow past an ellipsoid of revolution, and three dimensional flow through a curved square duct. Good agreement with published experimental and numerical data has been obtained. After the validation of the present procedure, techniques for acceleration were explored. It was found that the multigrid technique was efficient in reducing the CPU time needed for the simulation and improved the solution quality because of the lower residuals achieved. The GMRES does not work successfully presumably because of the diagonal algorithm used as the preconditioner.

The present multigrid iterative scheme for unsteady incompressible viscous flows is being extended to three-dimensions. The single-grid version has already been tested as discussed in Chapter IV. It is proposed that the following calculations be done to test the suitability of this procedure to three-dimensional viscous flows :

(a) Completion of three-dimensional multigrid solver validation for a curved square duct flow

(b) Application of the three-dimensional multigrid method to flow past a marine propeller (Fig.15) or a direct numerical simulation of the turbulent Rayleigh-Benard problem

(c) Extension to higher order accuracy in time. Specifically, the following studies will be done :

This is simple, and simply requires replacement of terms such as $(q^{n+1,k} - q^n) / \Delta t$ appearing in Eq.(3.9) to $(3 q^{n+1,k} - 4 q^n + q^{n-1}) / \Delta t$ etc. One can show this formally raises the time accuracy to $(\Delta t)^2$.

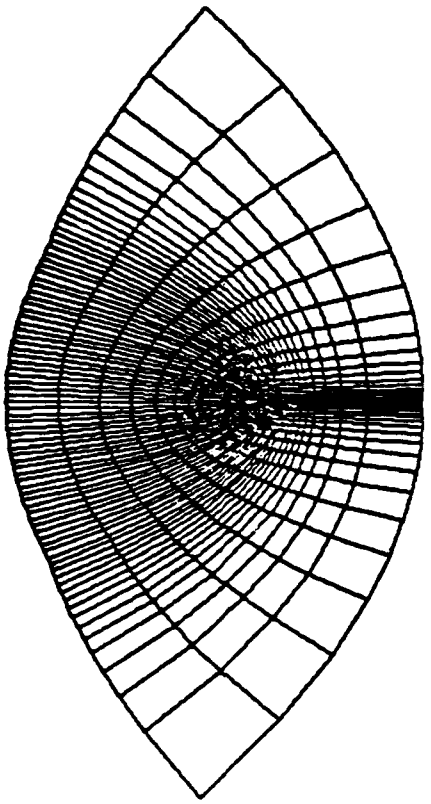

(a)

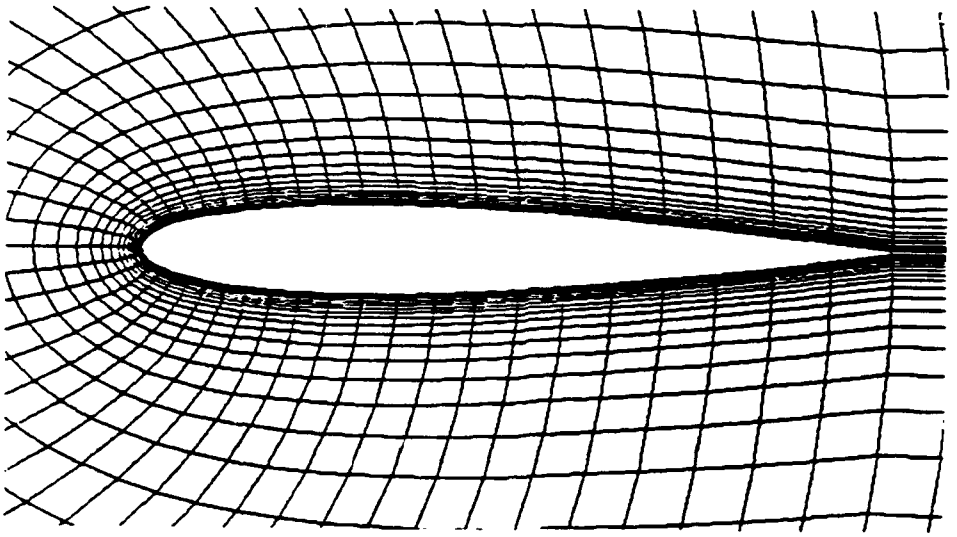

(b)

Figure 1. Body-Fitted Grid Around a NACA 0012 airfoil

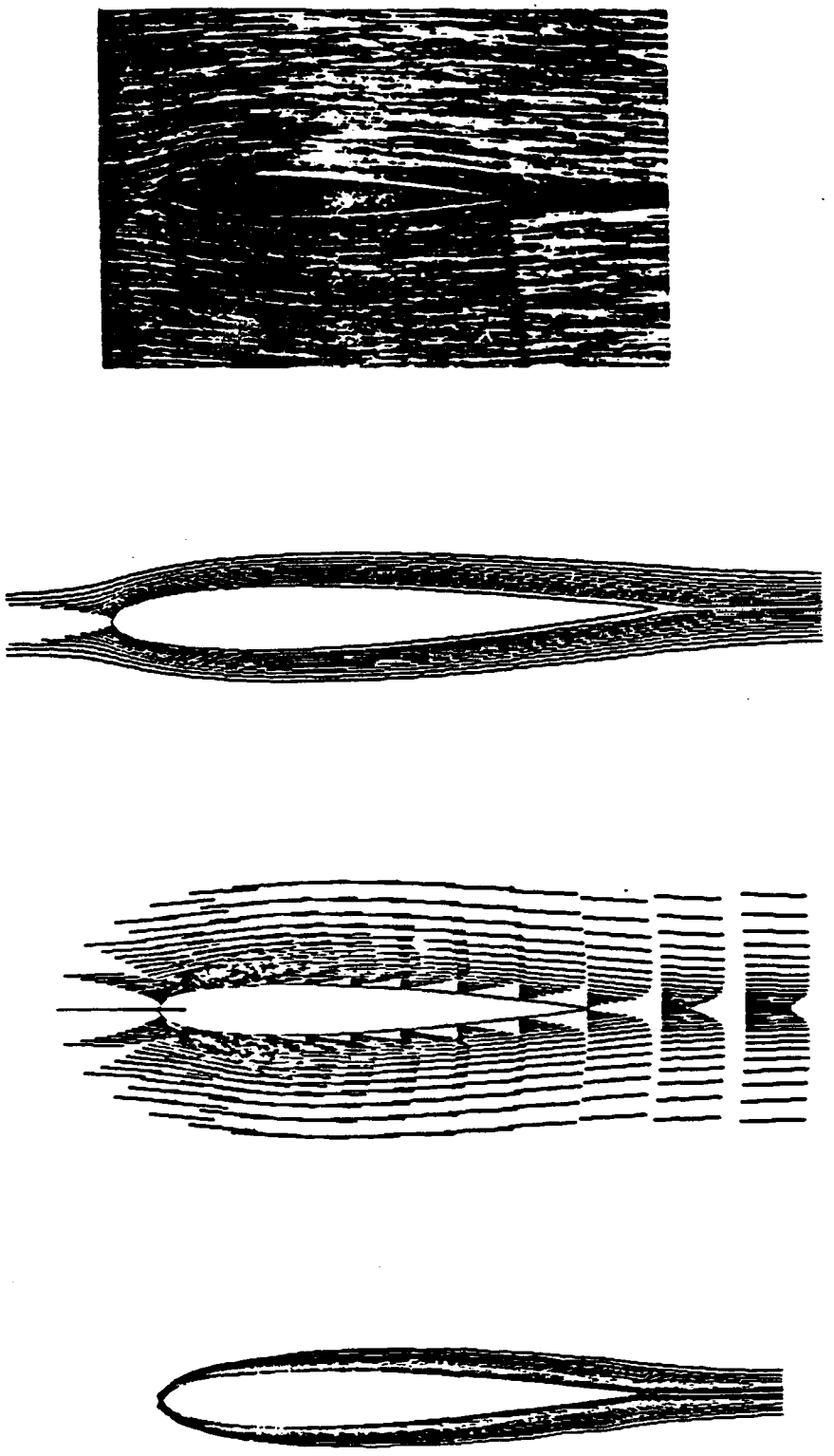

(a) $\alpha = 0$ (deg)

Figure 2. Instantaneous Streamlines, Velocity Profiles, and Vorticity Contours at Selected Angle of Attack with Experimental Flow Visualizations

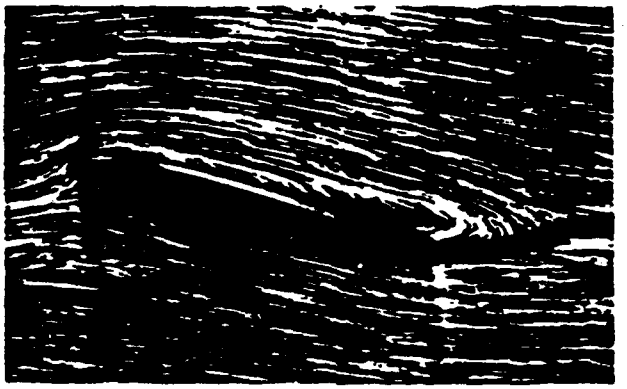

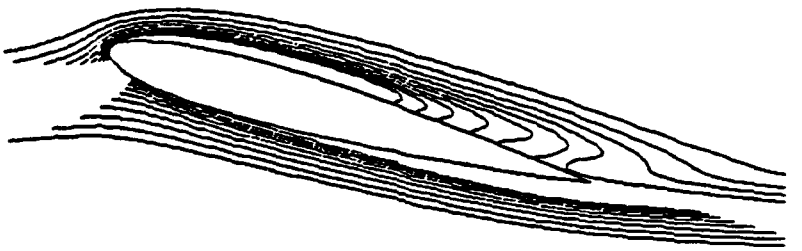

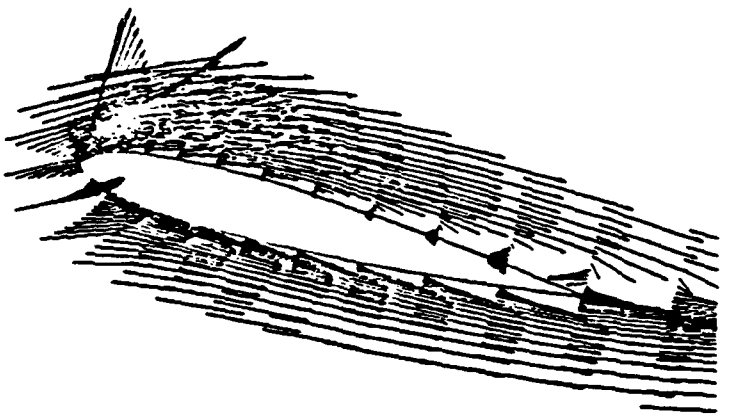

(b) $\alpha = 14.6$ (deg)

Figure 2. Continued..

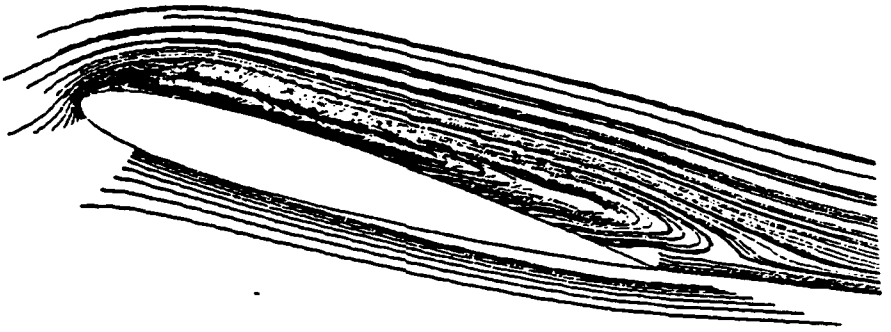

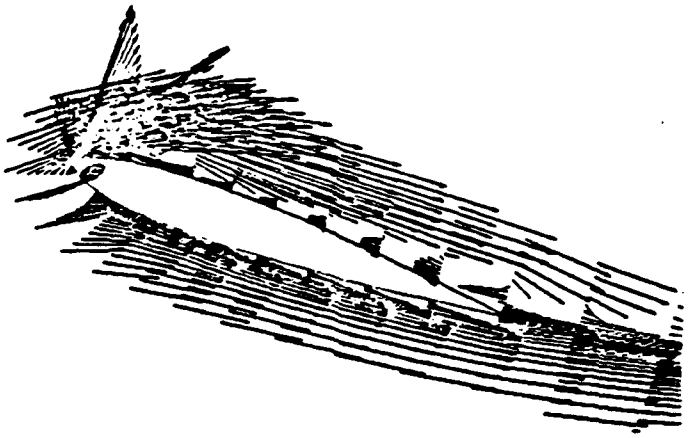

(c) $\alpha = 18.8$ (deg)

Figure 2. Continued.

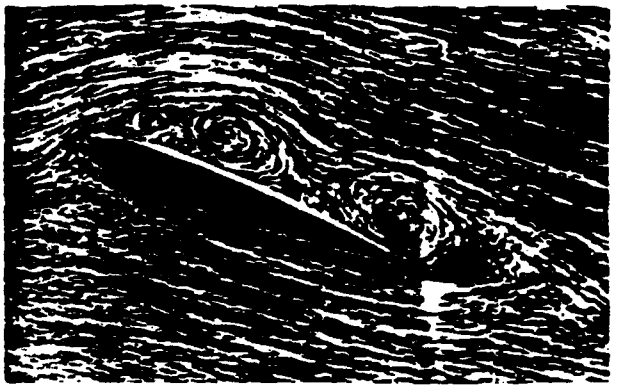

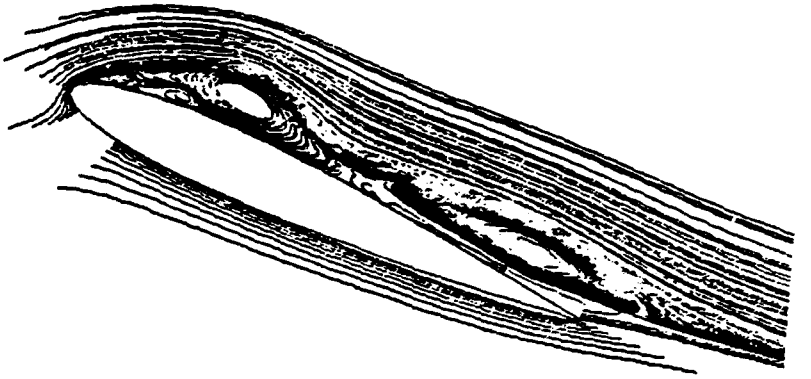

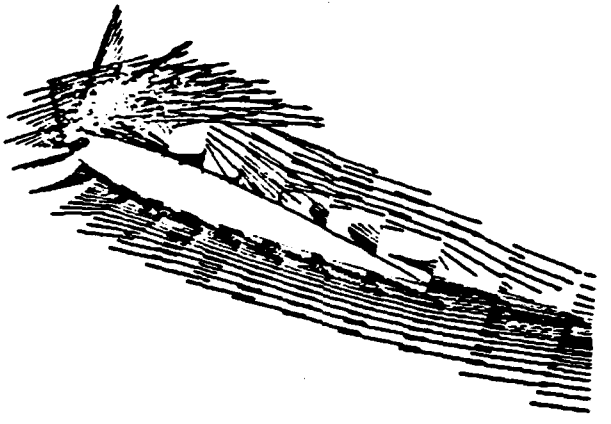

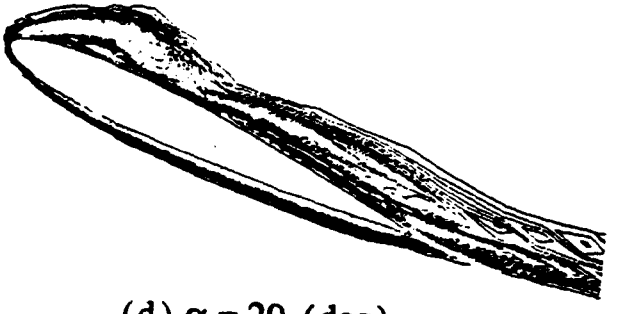

(d) $\alpha = 20$ (deg)

Figure 2. Continued.

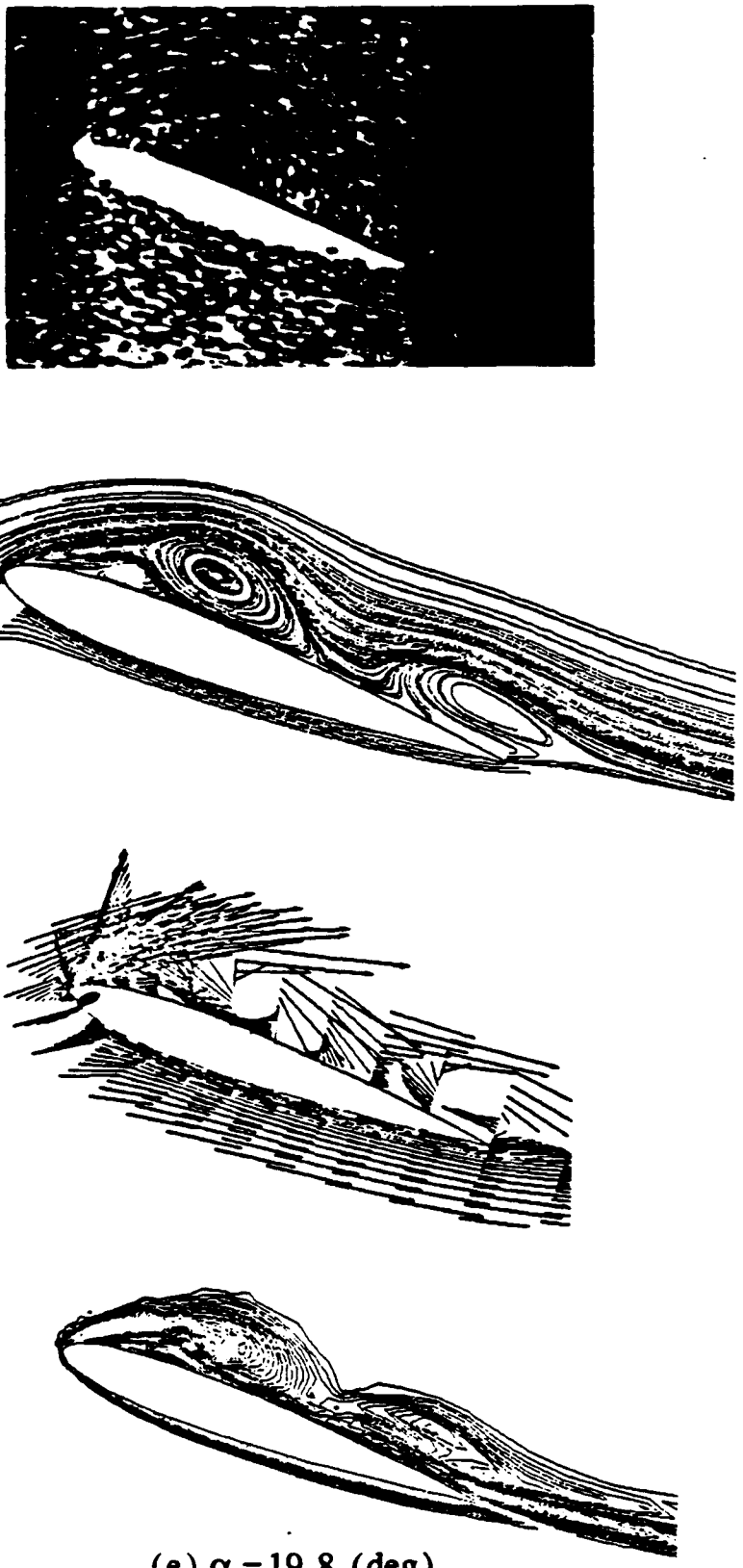

(e) $\alpha = 19.8$ (deg)

Figure 2. Continued.

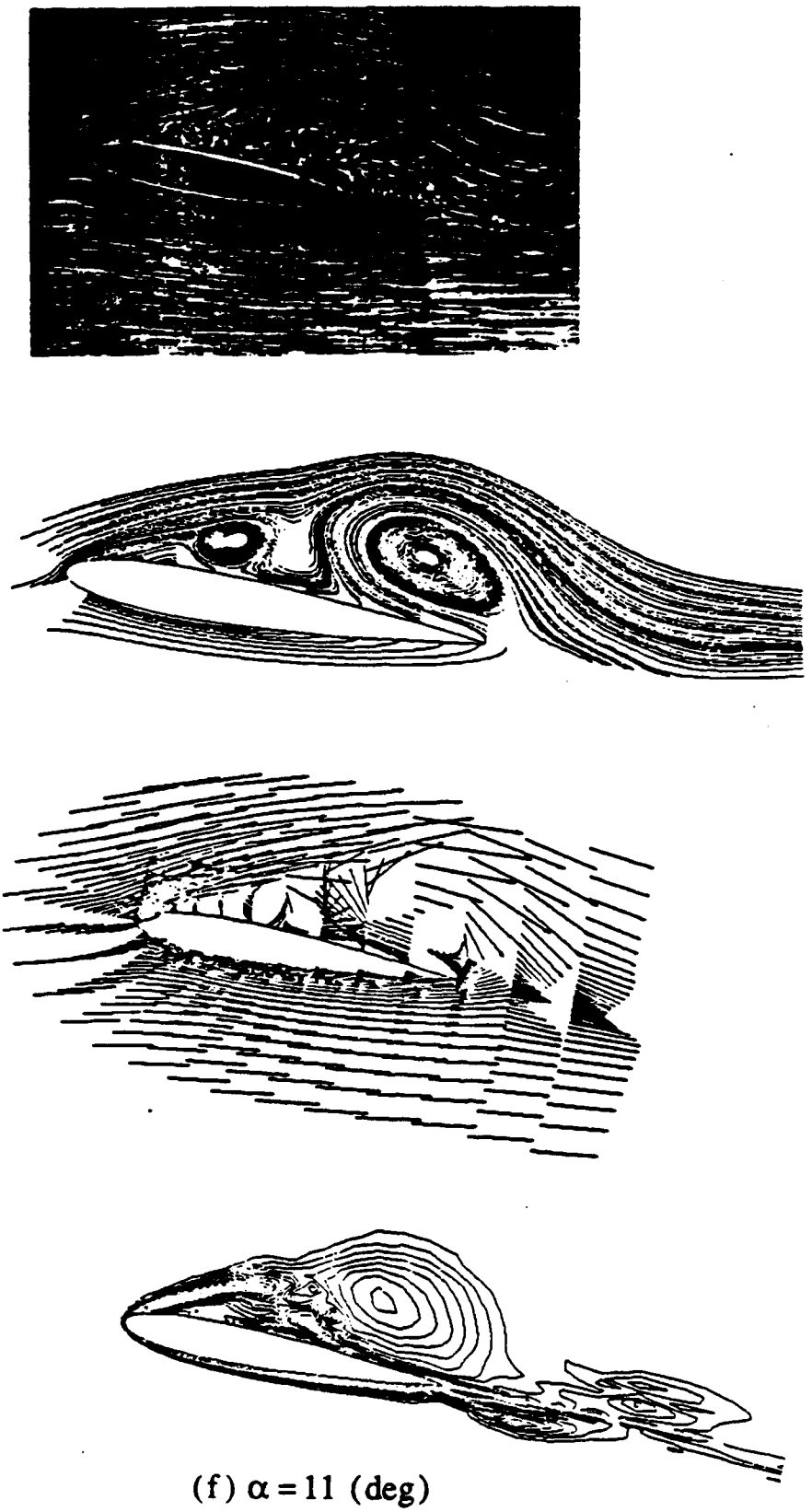

(f) $\alpha = 11$ (deg)

Figure 2. Continued.

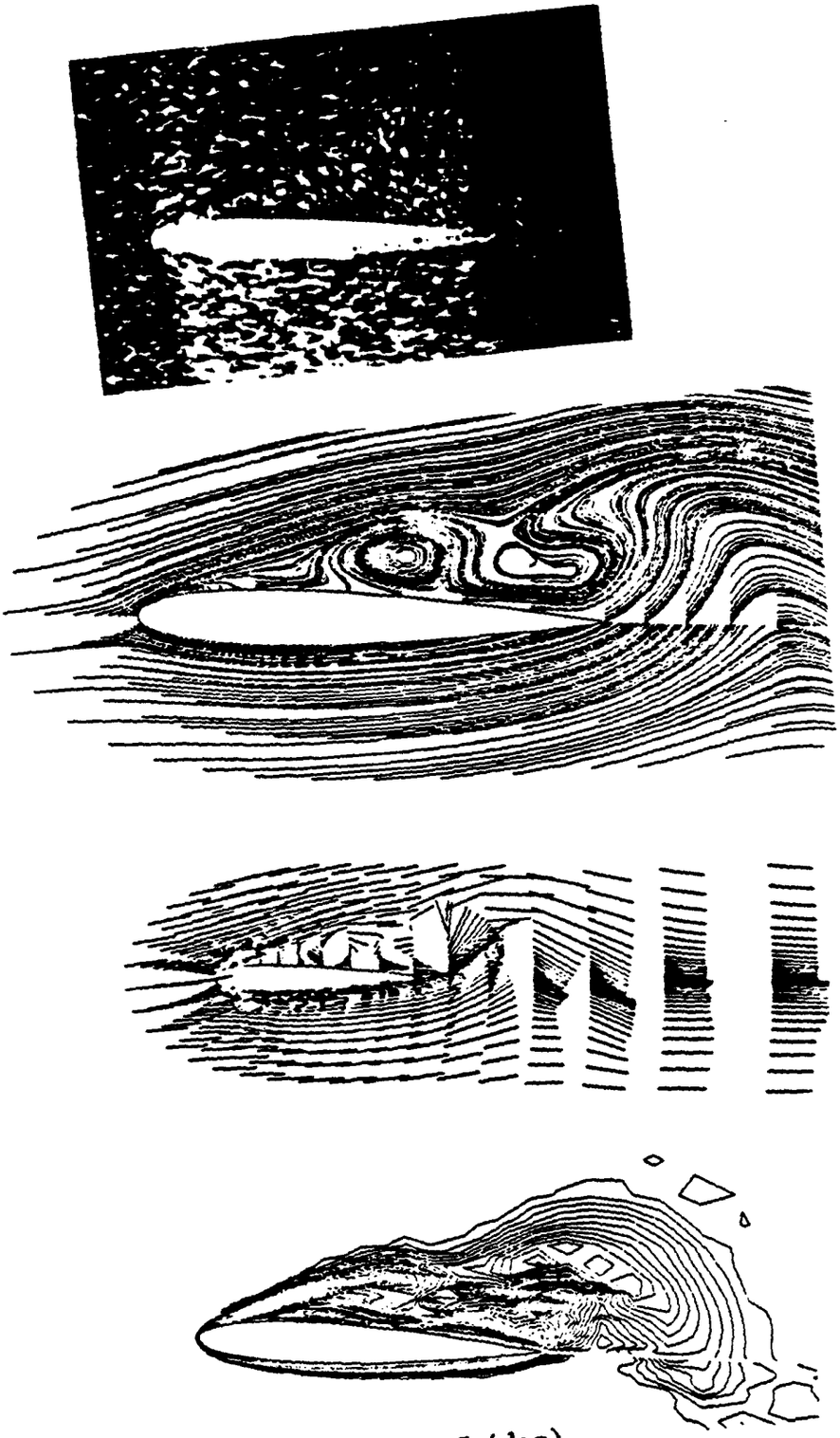

(g) $\alpha = 5$ (deg)

Figure 2. Continued.

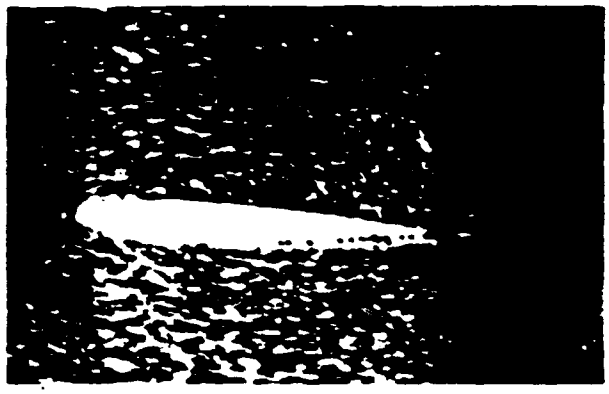

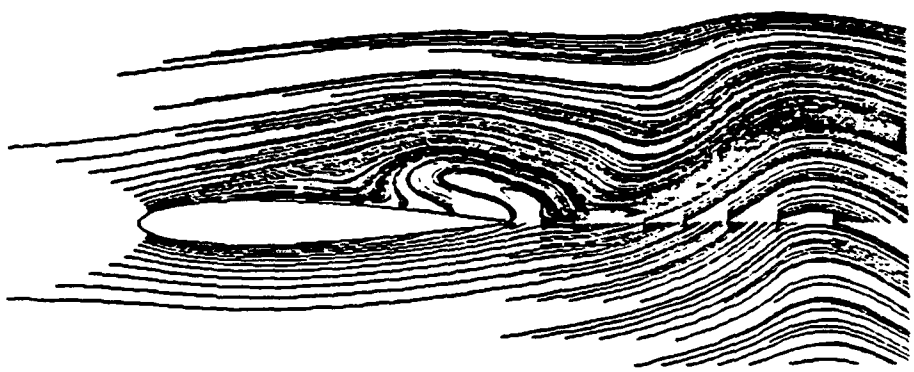

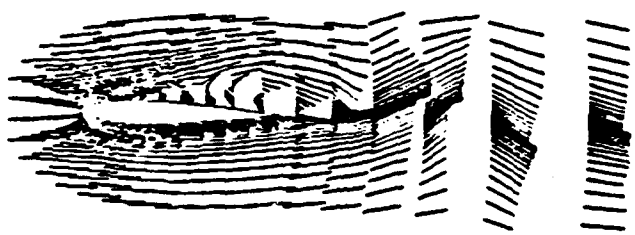

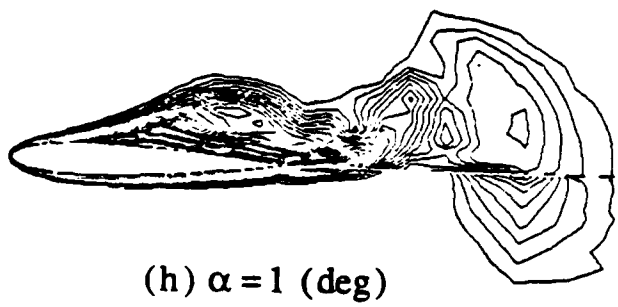

(h) $\alpha = 1$ (deg)

Figure 2. Continued.

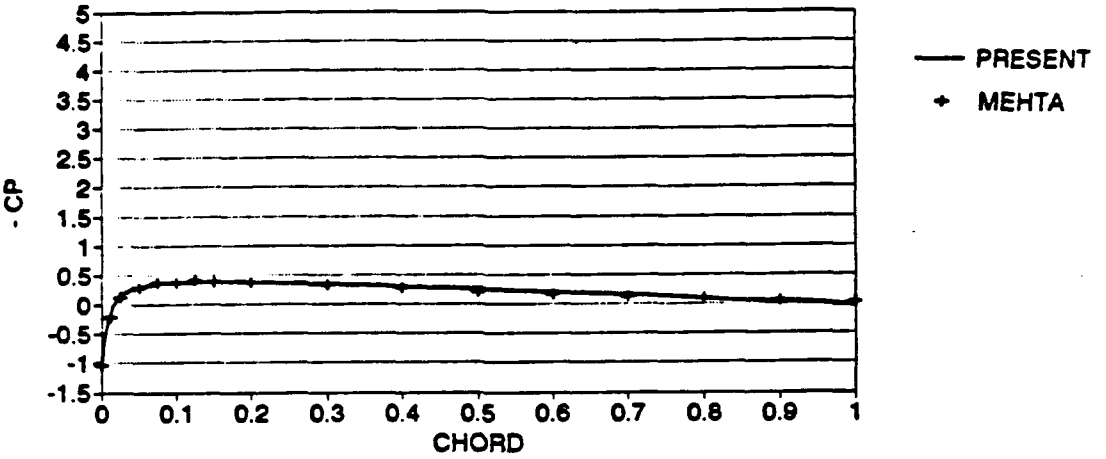

(a) $\alpha = 0$

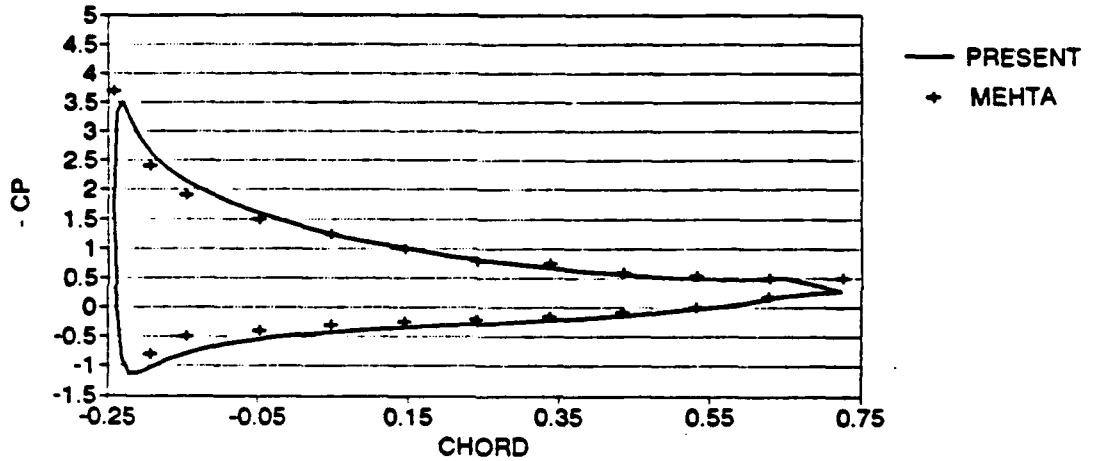

(b) $\alpha = 14.6$

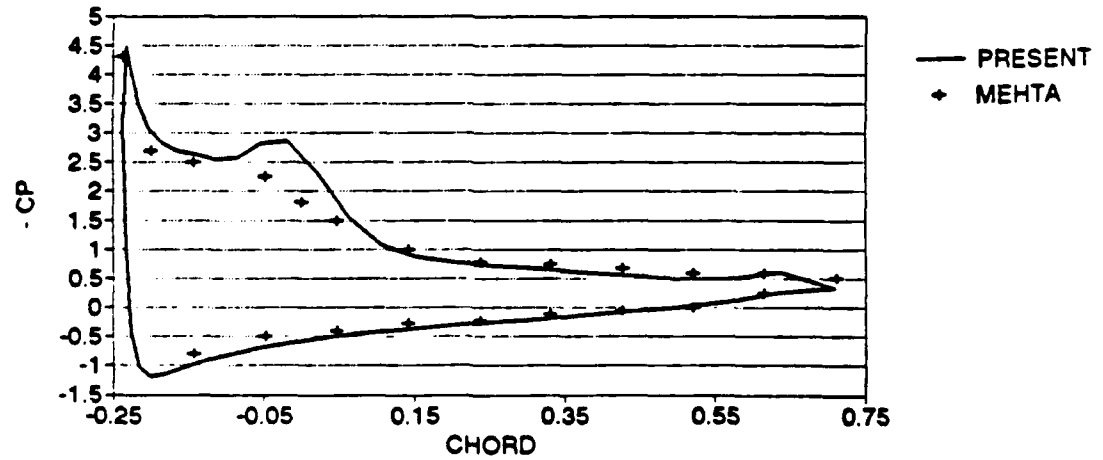

(c) $\alpha = 18.8$

Figure 3. Surface Pressure Distributions at Selected Angle of Attack

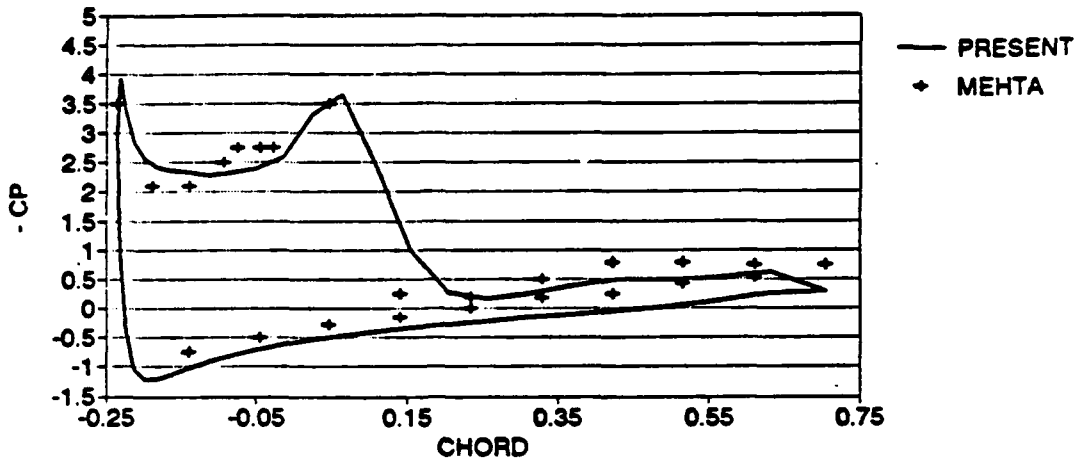

(d) $\alpha = 20$

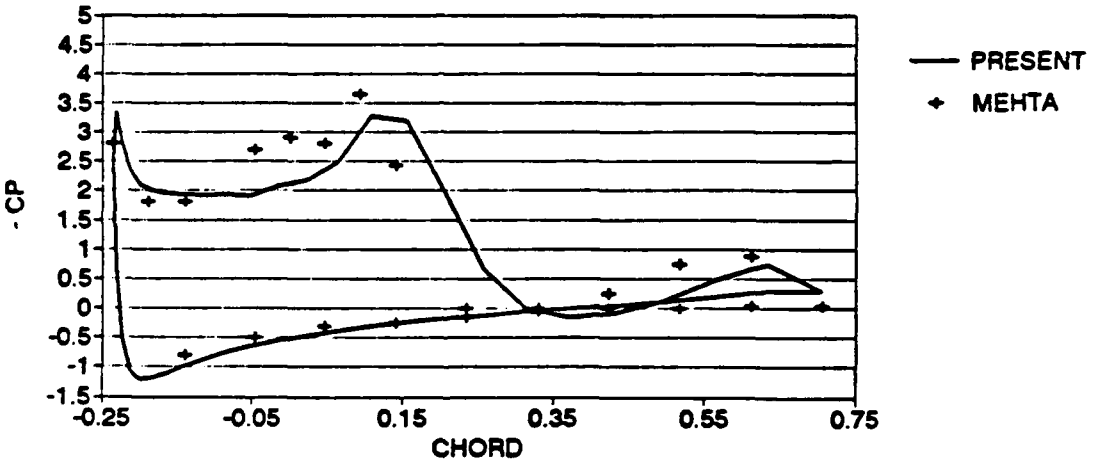

(e) $\alpha = 19.8$

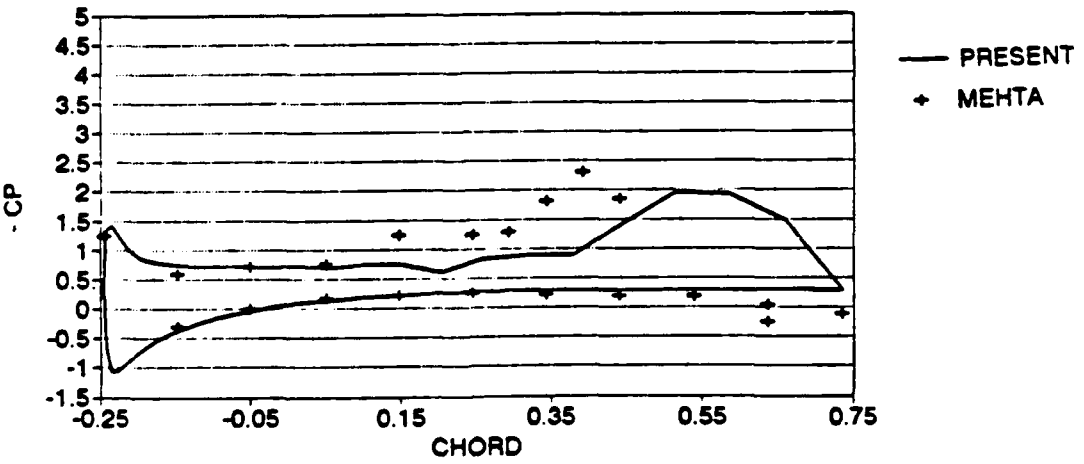

(f) $\alpha = 11$

Figure 3. Continued.

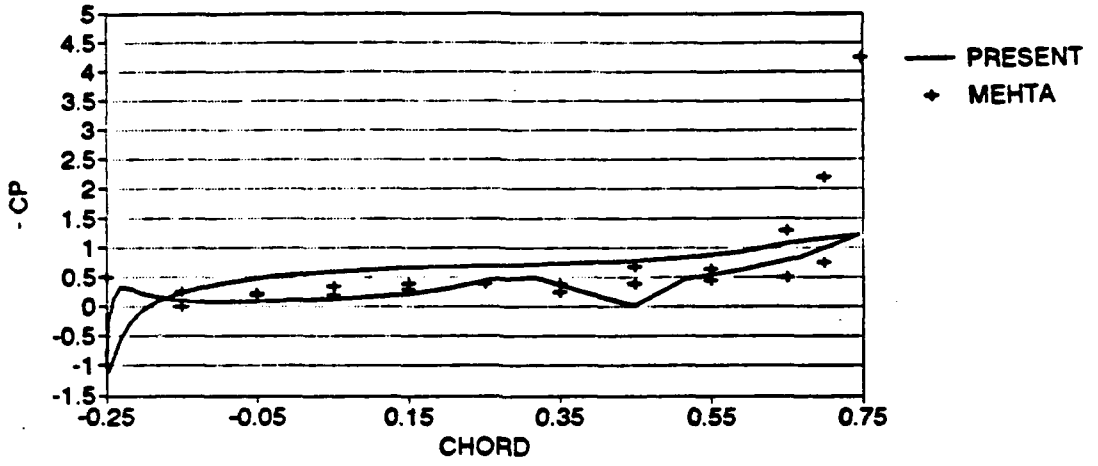

(g) $\alpha = 5$

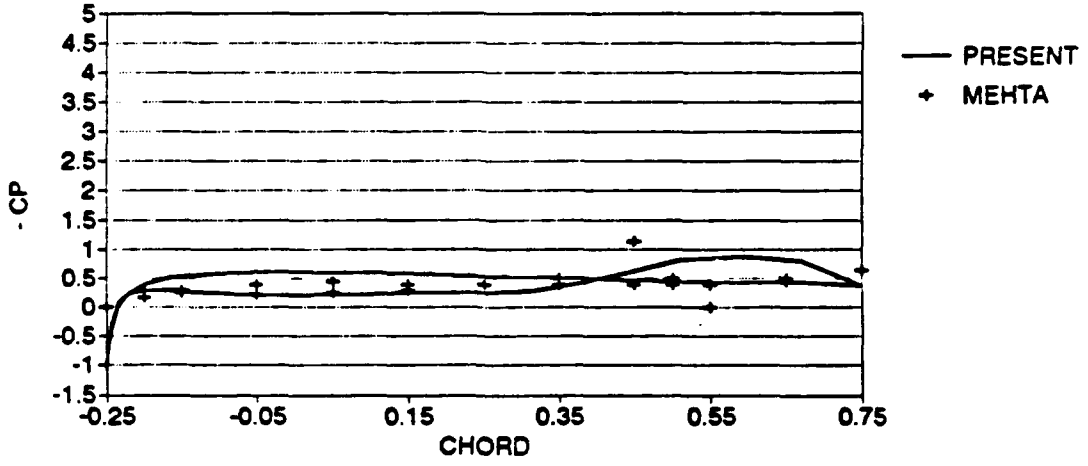

(h) $\alpha = 1$

Figure 3. Continued.

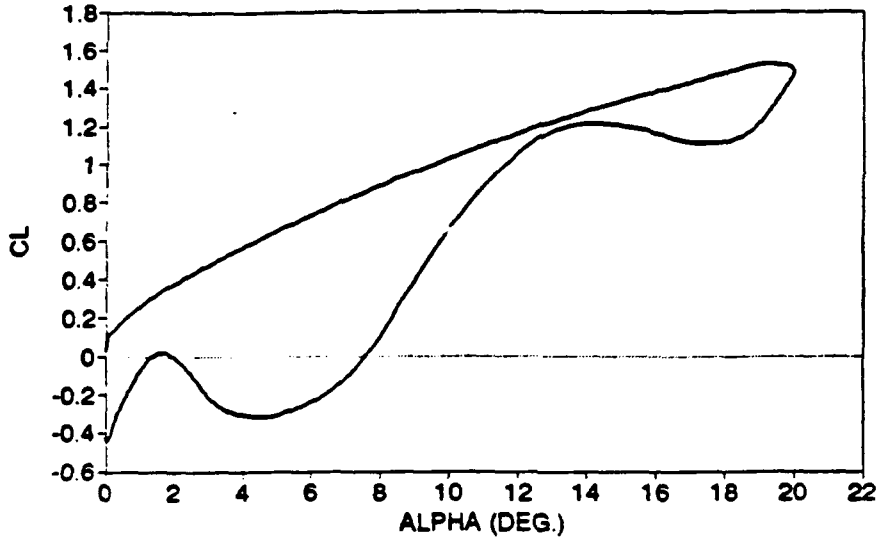

(a)

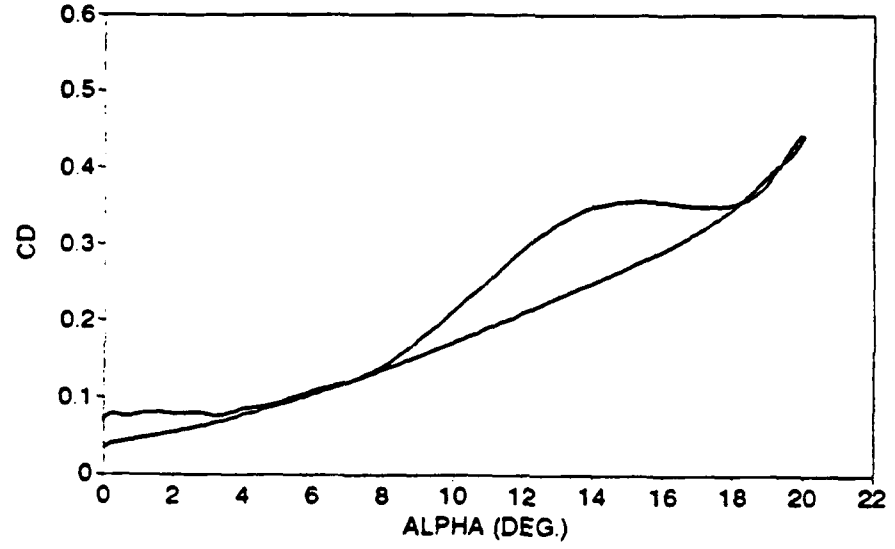

(b)

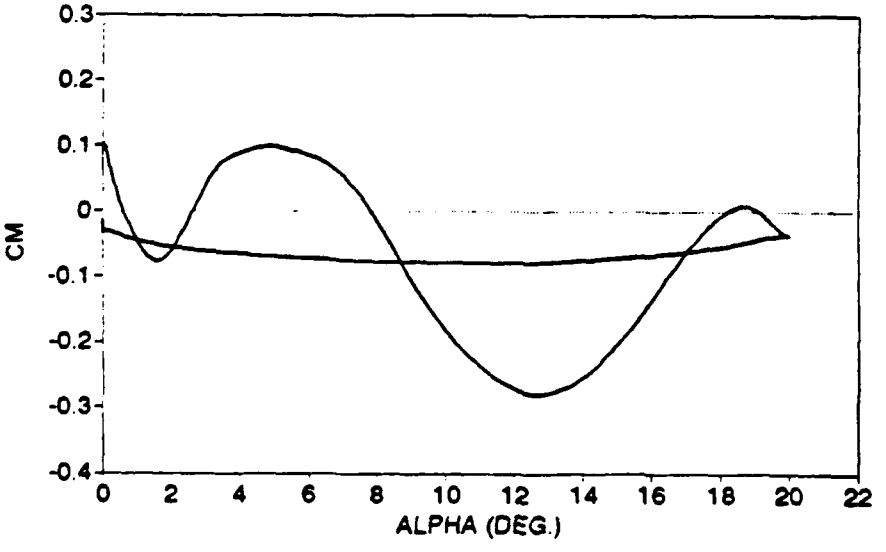

(c)

Figure 4. Dynamic Stall Hysteresis Loops for a NACA 0012 Airfoil

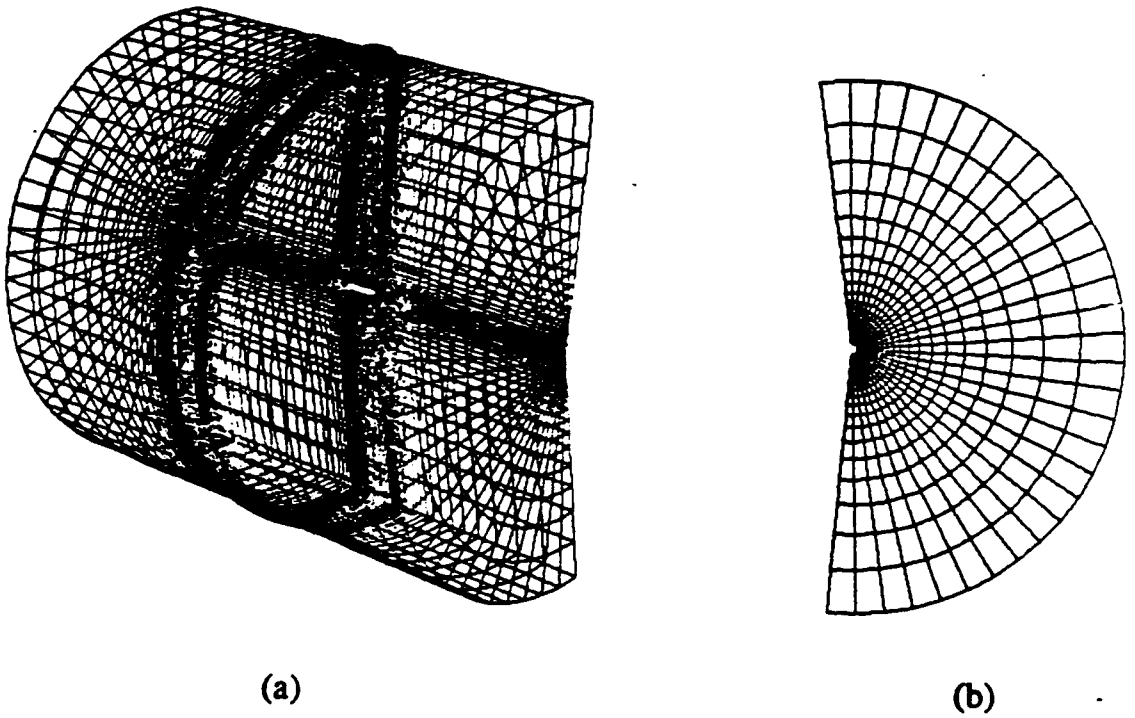

(a) (b)

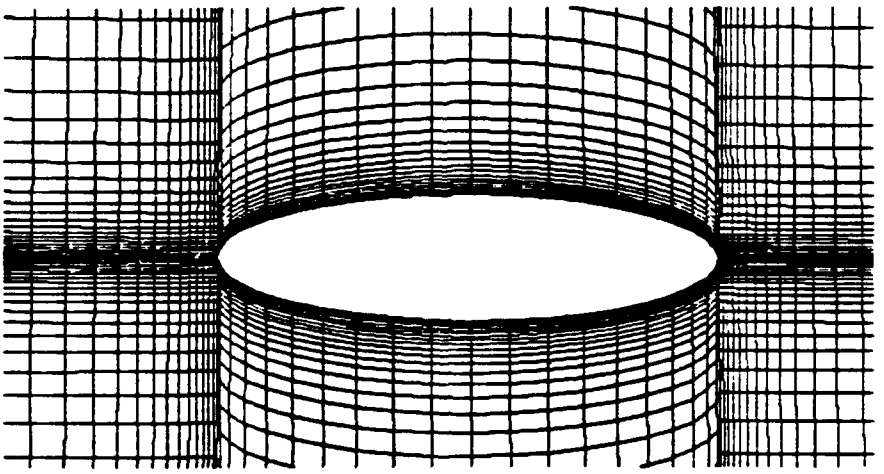

(c)

Figure 5. Body-Fitted Grid Around an Ellipsoid of Revolution

Figure 6. Streamlines over the Ellipsoid of Revolution

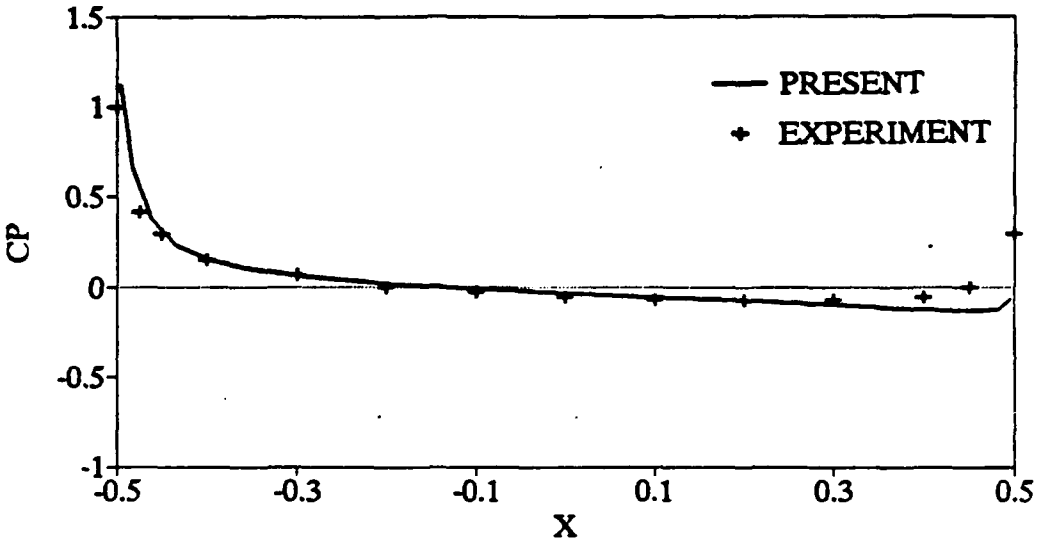

(a) In The Windard Plane

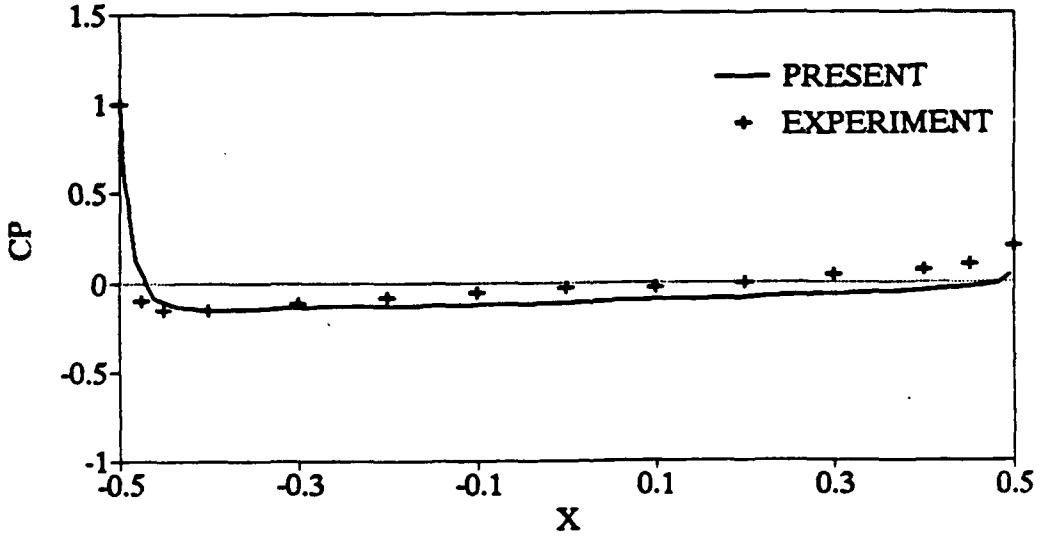

(b) In The Leeward Plane

Figure 7. Surface Pressure Distributions Compared With Experimental Data

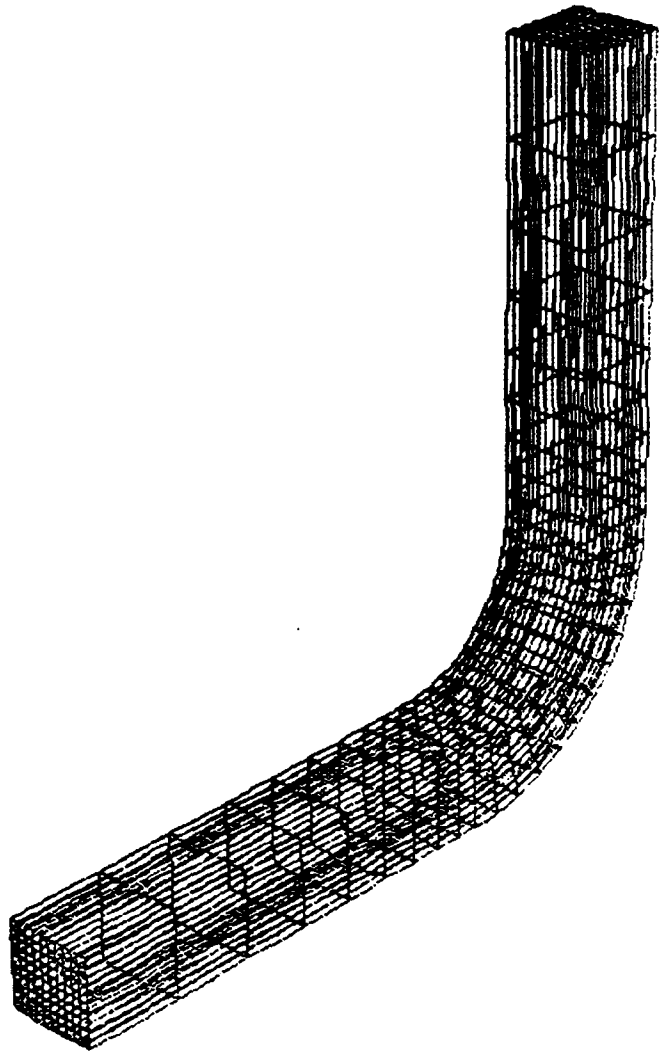

Figure 8. Body-fitted grid within a square duct with a 90-deg bend.

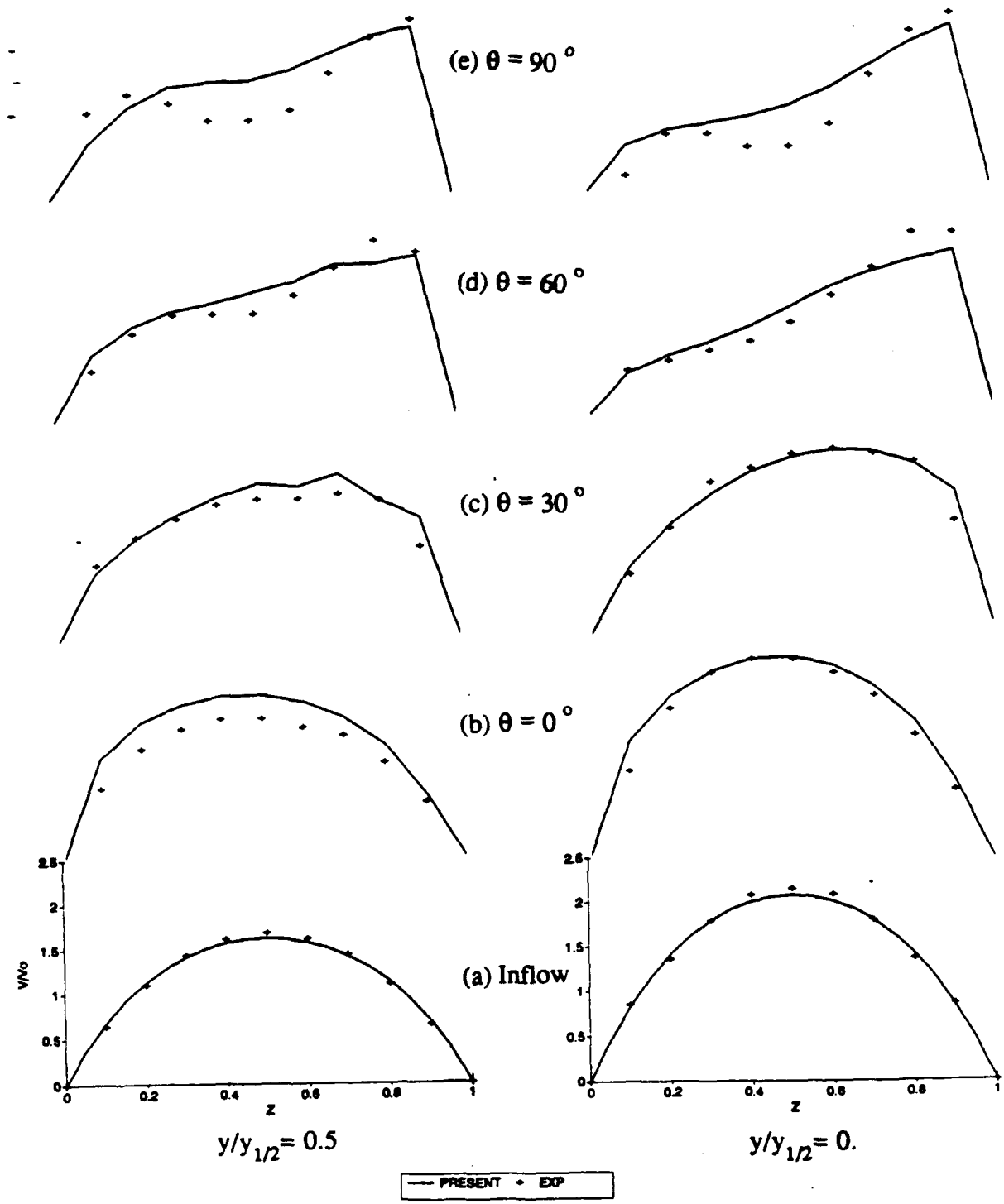

Figure 9. Streamwise velocity profiles compared with experiments.

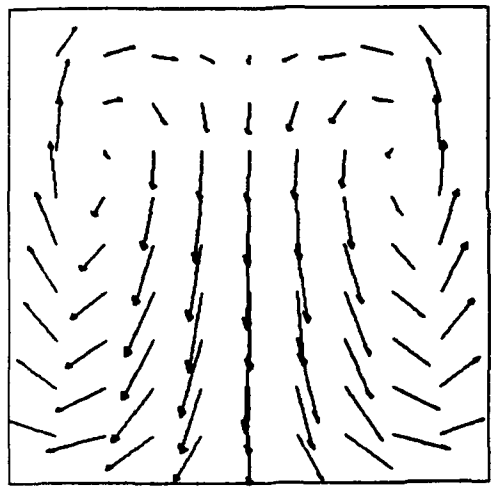

(a) $\theta = 30°$

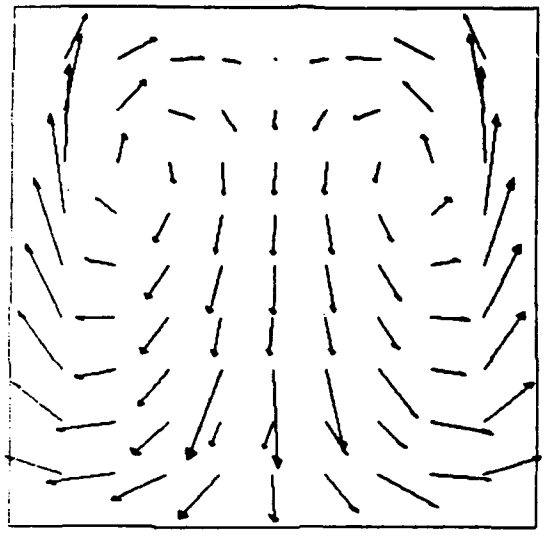

(b) $\theta = 60°$

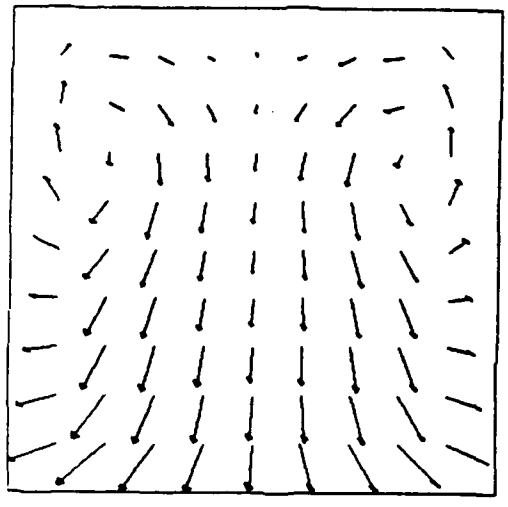

(c) $\theta = 90°$

Figure 10. Cross-sectional velocity profiles at three streamwise stations in the curved section.

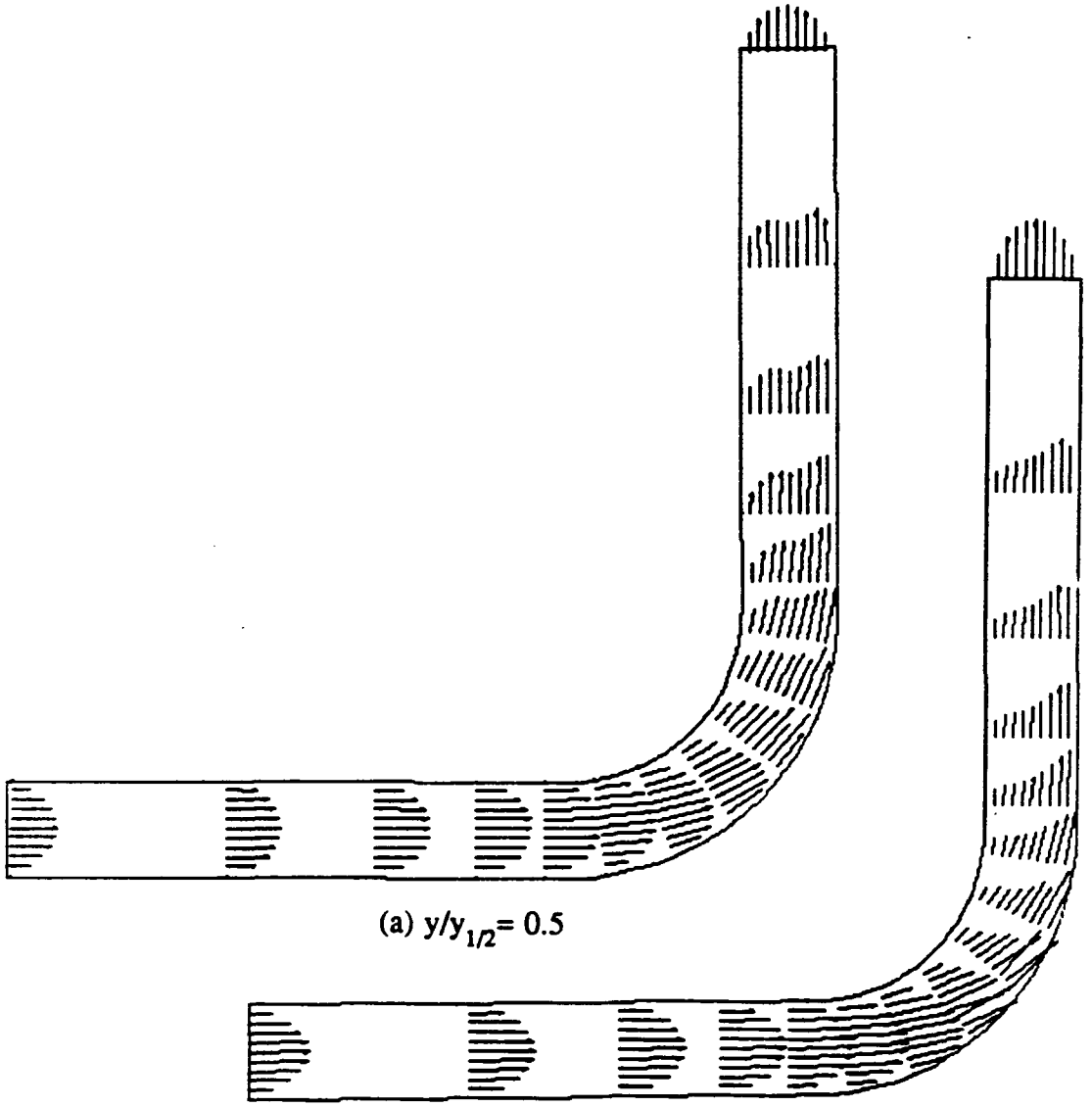

Figure 11. Streamwise velocity profiles at $y/y_{1/2}$= 0.5 and $y/y_{1/2}$= 0.

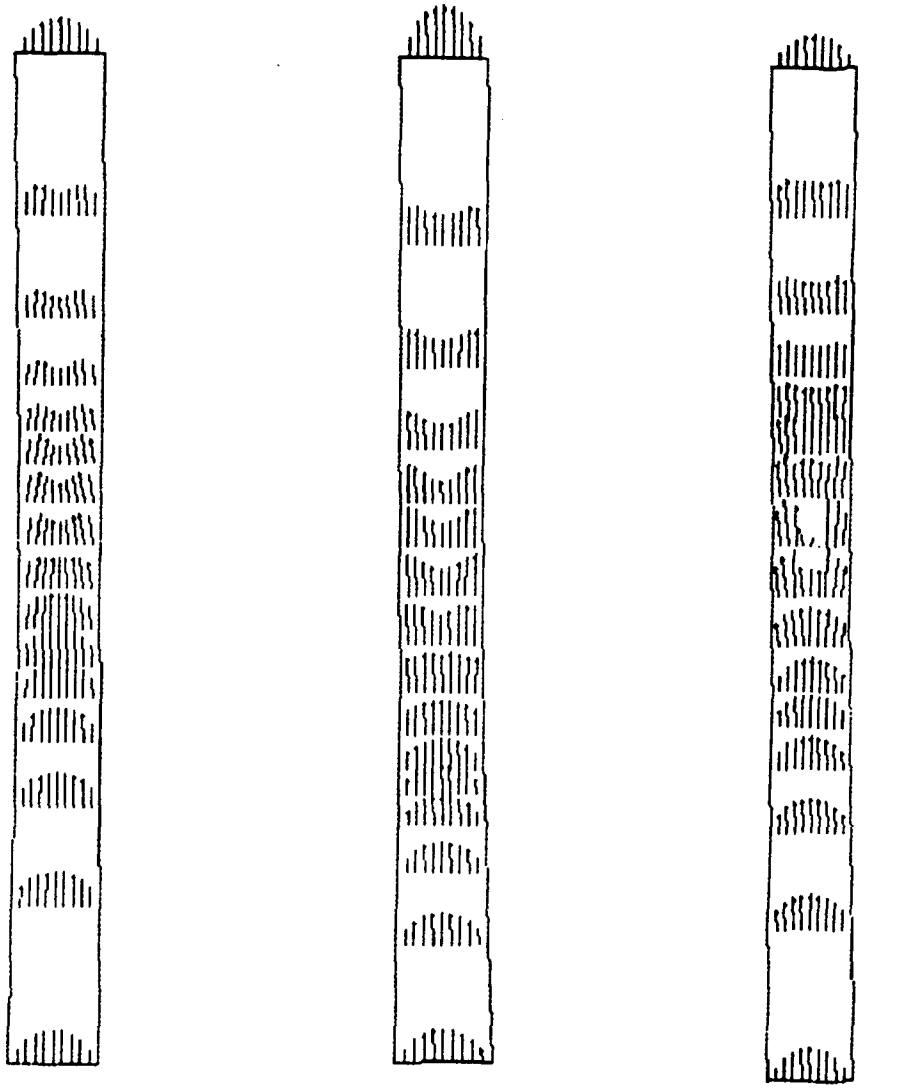

(a) z = 0.25 (b) z = 0.5 (c) z = 0.75

Figure 12. Streamwise velocity profiles at z = 0.25, z = 0.5 and z = 0.75.

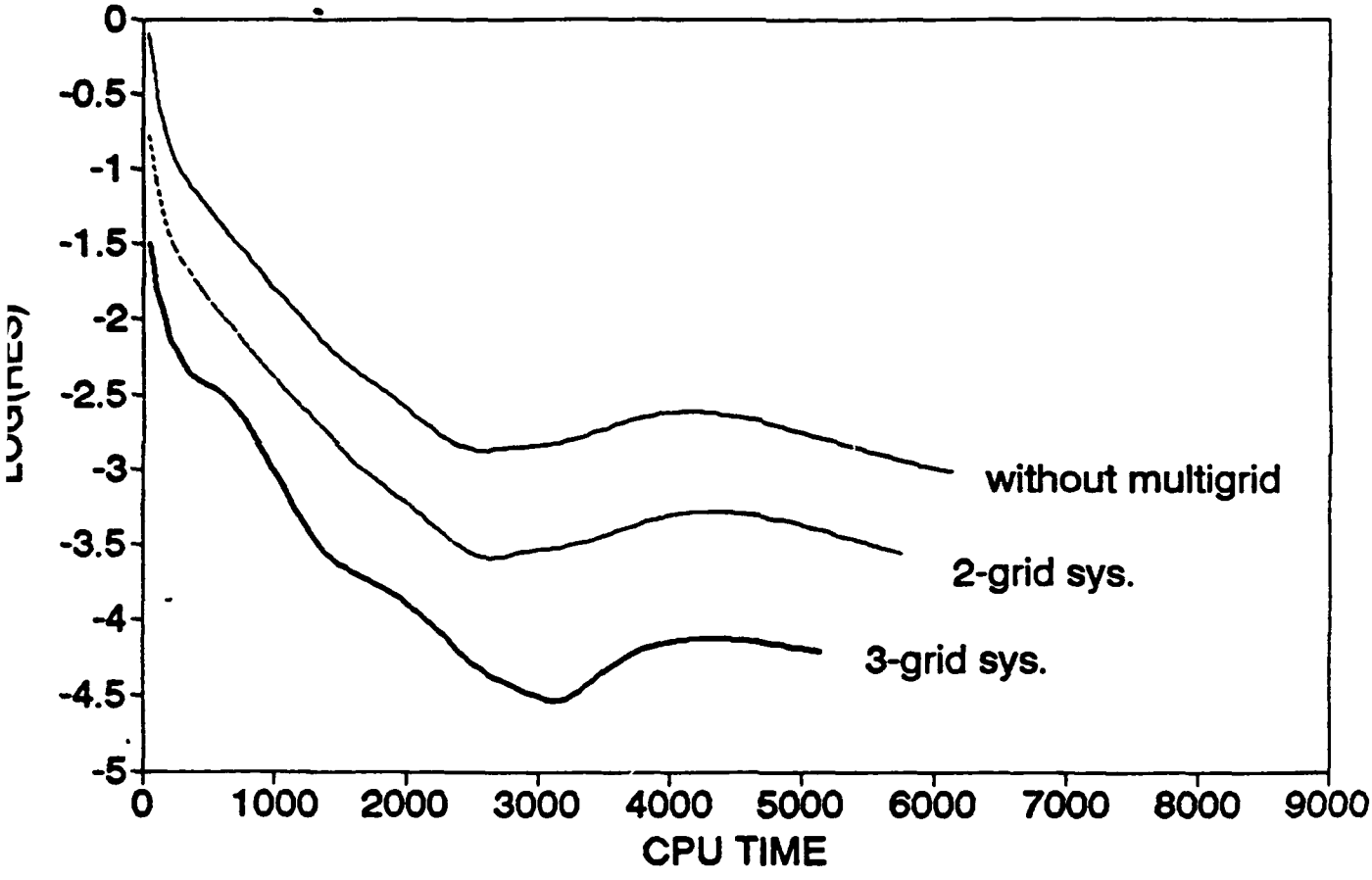

Figure 13. Comparison of Convergence History of NACA 0012 Airfiol for Steady State (at Zero Degree Angle of Attack)

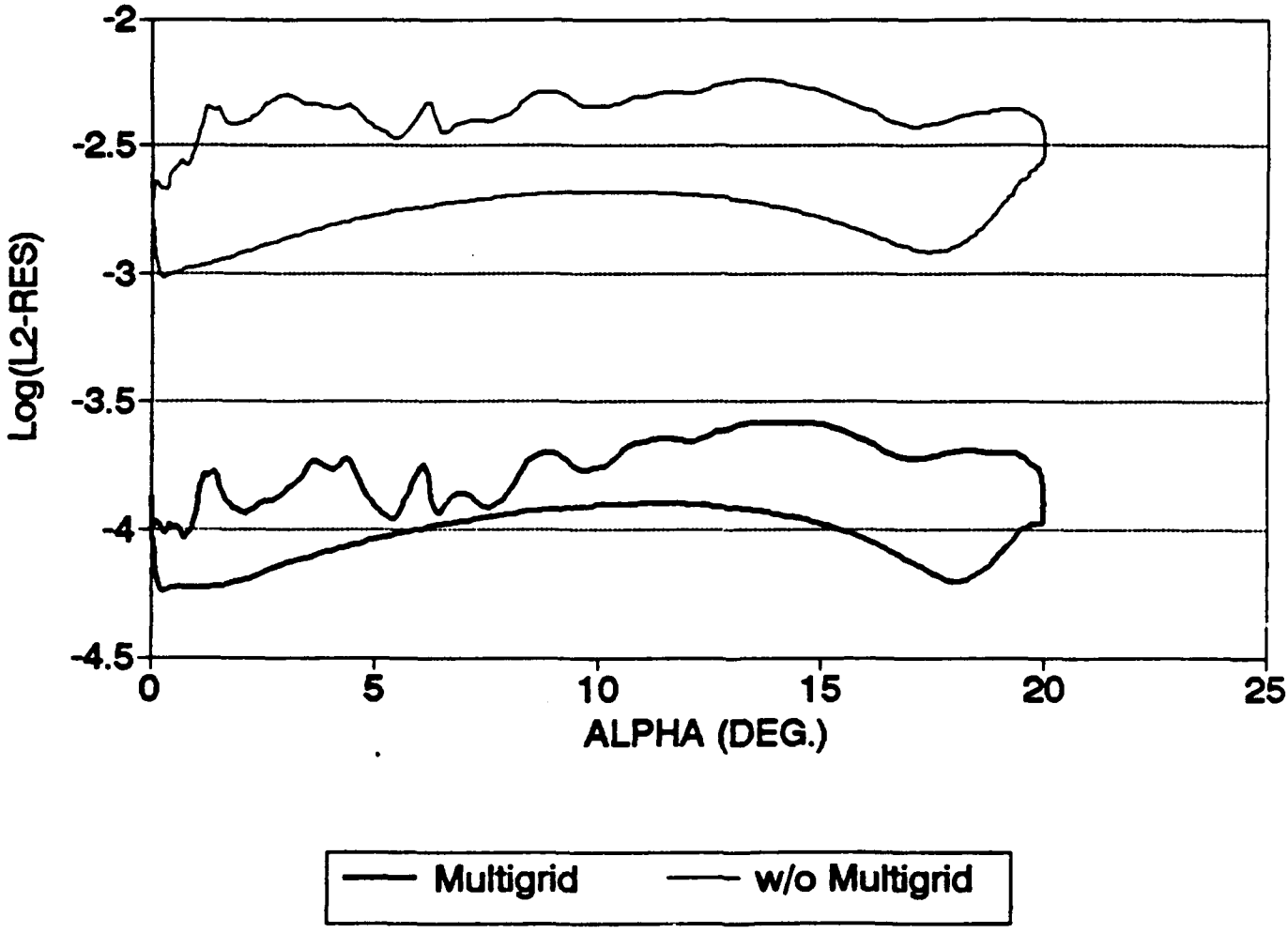

Figure 14. Comparison of Global Residual History of a Sinusoidally Oscillating Airfoil

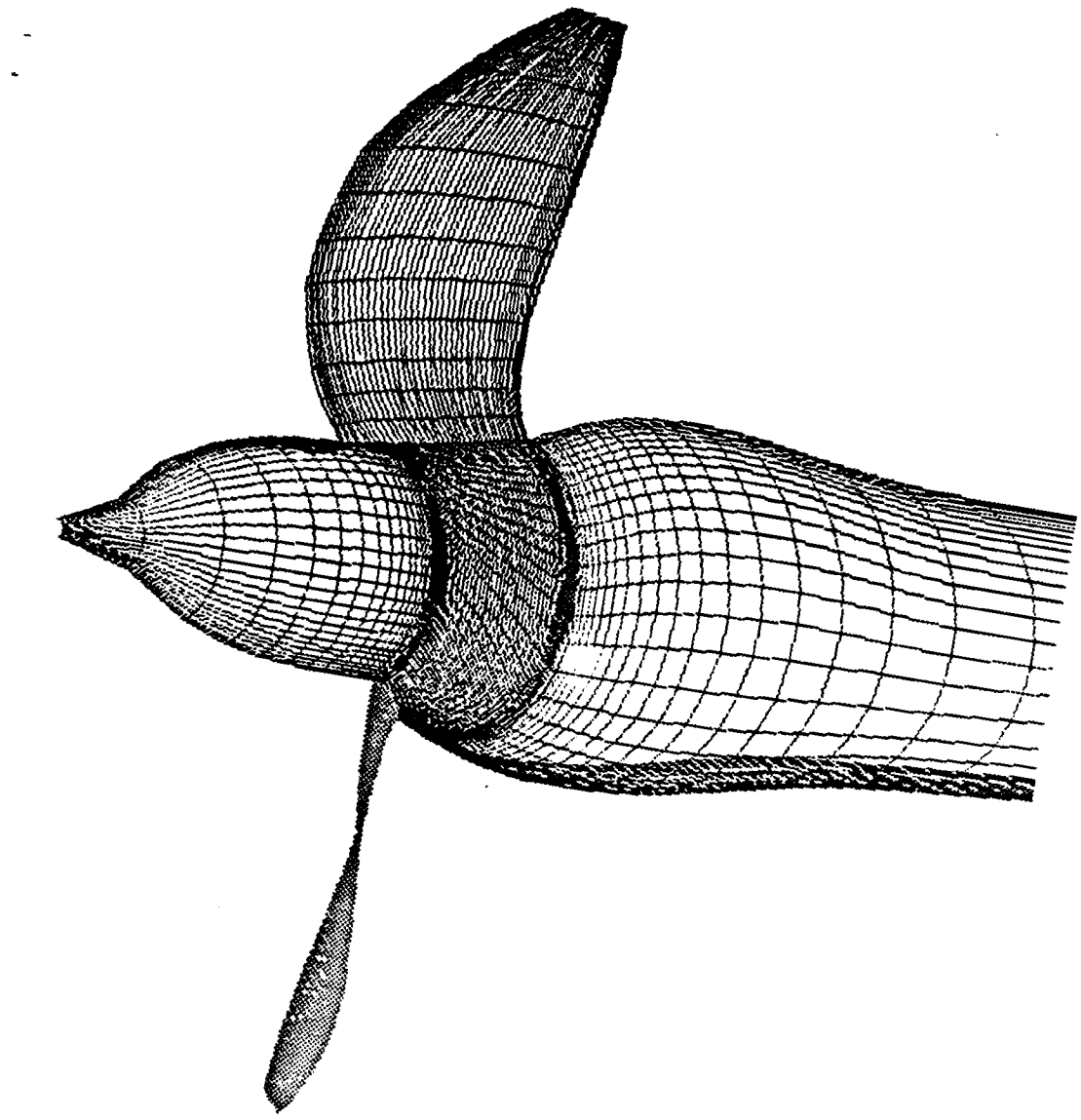

Figure 15. Configuration of Marine Propeller
(2-Bladed SR7L)

REFERENCES

1. Gresho, P. M. and Sani, R. L.,"On Pressure Boundary Conditions for the Incompressible Navier-Stokes Equations," International Journal for Numerical Methods in Fluids, Vol. 7, 1987, pp.1111-1145.
2. Anderson, D. A., Tannehill, J. C. and Pletcher, R. H., Computational Fluid Mechanics and Heat Transfer, Hemisphere Publishing, N.Y., 1984.
3. Mehta, U. B.,"Dynamic Stall of an Oscillating Airfoil," AGARD CP-227, 1977.
4. Wu, J. C.,"Numerical Boundary Conditions for Viscous Flow Problems," AIAA Journal, Vol. 14, No. 8, 1976, pp.1042-1049.
5. Thames, F. C.,"Numerical Solution of Incompressible Navier-Stokes Equations About Arbitrary Two-Dimensional Bodies," Ph. D. Thesis, Mississippi State University, Mississippi, August, 1977.
6. Harlow, F. H. and Welch, J. E.,"Numerical Calculation of Time-Dependent Viscous Incompressible Flow with Free Surfaces," Physics of Fluids, Vol. 8, No. 12, 1965, pp.2182-2185.
7. Osswald, G. A., Ghia, K.N. and Ghia, U.,"An Implicit Time Marching Method for Studying Unsteady Flow with Massive Separation," AIAA CP-854, 1985, pp.686-696.
8. Goda, K.,"Multistep Implicit Technique with Implicit Difference Schemes for Calculating Two- or Three-Dimensional Cavity Flows," Journal of Computational Physics, Vol. 30, 1979.
9. Abdallah, S.,"Numerical Solutions for the Incompressible Navier-Stokes Equations in Primitive Variable Using a Non-Staggered Grid, II," Journal of Computational Physics, Vol. 70, 1987, pp.193-202.
10. Mansour, M. L. and Hamed, A.,"Implicit Solution of the Incompressible Navier-Stokes Equations on a Non-Staggered Girds,"Journal of Computational Physics, Vol. 86, 1990, pp.147-167.
11. Viecelli, J. A.,"A Method for Including Arbitrary External Boundaries in the MAC Incompressible Fluid Computing Technique,"Journal of Computational Physics, Vol. 4, 1969, pp.543-551.

12. Hirt, C. W. and Cook, J. L.,"Calculating Three-Dimensional Flows Around Structures and Over Rough Terrain,"Journal of Computational Physics, Vol. 10, 1972, pp.324-340.
13. Chorin, A. J.,"Numerical Solution of Navier-Stokes Equations," Mathematics of Computation, Vol. 22, 1968, pp.745-762.
14. Steger, J. L. and Kutler,P.,"Implicit Finite-Difference Procedures for the Computation of Vortex Wakes," AIAA Journal, Vol. 15, 1977, pp.581-590.
15. Kwak, D., Chang, J. L. C., Shanks, S. P. and Chakravarthy, S. R.,"A Three-Dimensional Incompressible Navier-Stokes Flow Solver Using Primitive Variables," AIAA Journal, Vol. 24, 1986, pp.390-396.
16. Chorin, A. J.,"A Numerical Method for Solving Incompressible Viscous Flow Problems," Journal of Computational Physics, Vol. 2, 1967, pp.12-26.
17. Beam, R. M. and Warming, R. F.,"An Implicit Finite-Difference Algorithm for Hyperbolic Systems in Conservative-Law Form," Journal of Computational Physics, Vol. 22, 1976, pp.87-110.
18. Merkle, C. L. and Athavale, M.,"Time-Accurate Unsteady Incompressible Flow Algorithms Based on Artificial Compressibility," AIAA Paper 87-1137, June 1987.
19. Rogers, S. E. and Kwak, D.,"Steady and Unsteady Solutions of the Incompressible Navier-Stokes Equations," AIAA Journal Vol. 29, No. 4, 1991, pp.603-610.
20. Shih, T. M., Tan, H and Hwang, B. C.,"Equivalence of Artificial Compressibility Method and Penalty-Function Method," Numerical Heat Transfer, Part B, Vol. 15, 1989, pp.127-130.
21. Leonard, B. P.,"A Stable and Accurate Convective Modelling Procedure Based on Quadratic Upstream Interpolation," Computer Methods in Applied Mechanics and Engineering, Vol. 19, 1979, pp.59-98.
22. Michelassi, V. and Benocci, C.,"Prediction of Incompressible Flow Separation with the Approximate Factorization Technique," International Journal for Numerical Methods in Fluids, Vol. 7, 1987, pp.1383-1403.
23. Biringen, S. and Cook, C.,"On Pressure Boundary Conditions for the Incompressible Navier-Stokes Equations Using Nonstaggered Grids," Numerical Heat Transfer, Vol. 3, 1988, pp.241-252.
24. Werlé, H.,"Hydrodynamic Flow Visualization," Annual Review of Fluid Mechanics, Vol. 5, 1973, pp.361-382.
25. Patel, V. C. and Baek, J. H.,"Boundary Layers in Planes of Symmetry, Part II : Calculations for Laminar and Turbulent Flows," AIAA Journal, Vol. 25, No. 6, 1987, pp.812-818.
26. Meier, H. U. and Kreplin, H. D.,"Experimental Investigation of Boundary Layer Transition and Separation on a Body of Revolution," Zeitscriff für Flugwiss

27. Humphrey, J. A. C., Taylor, A. M. K. and Whitelaw, J.H.," Laminar Flow in a Square Duct of a Strong Curvature," Journal of Fluid Mechanics, Vol.83, 1977, pp.590-527.

28. White, F. M. Viscous Fluid Flow, McGraw-Hill, 1974, pp.120.